© 2018. Published by The Company of Biologists Ltd | Development (2018) 145, dev169722. doi:10.1242/dev.169722

CORRECTION

Correction: Amniotic ectoderm expansion in mouse occurs via distinct modes and requires SMAD5-mediated signalling (doi: 10.1242/dev.157222)

Mariya P. Dobreva, Vanesa Abon Escalona, Kirstie A. Lawson, Marina N. Sanchez, Ljuba C. Ponomarev, Paulo N. G. Pereira, Agata Stryjewska, Nathan Criem, Danny Huylebroeck, Susana M. Chuva de Sousa Lopes, Stein Aerts and An Zwijsen

There were errors in Development (2018) **145**, dev157222 (doi: 10.1242/dev.157222).

On p.1, the sentence should read 'This causes amnion-chorion separation and results in three cavities at E7.5: the amniotic and ectoplacental cavities, and the *de novo*-derived exocoelomic (visceral yolk sac) cavity.'

Fig. 1 and its legend contained an error. The correct figure and legend are provided below.

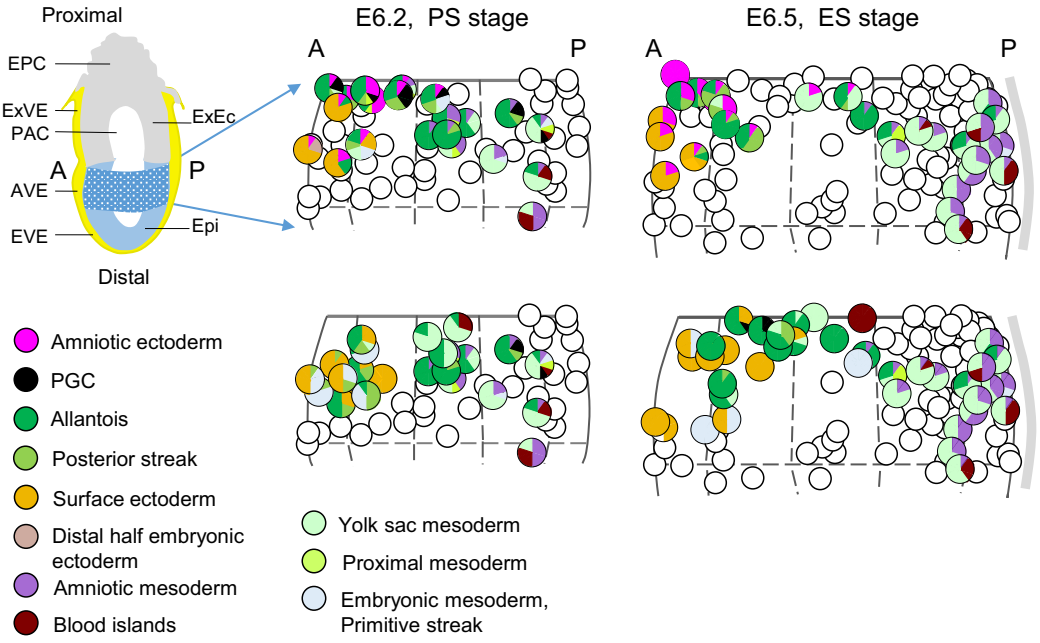

Fig. 1. Amnion fate map. Fate maps of amniotic ectoderm and amniotic mesoderm. Top left: cartoon of a midsagittal section of an E6.2, prestreak stage (PS) embryo. The proximal half of the epiblast cup (blue pattern) is expanded in the right panels and projected on the sagittal midline of PS and early-streak (ES) stages. Left and right halves of the epiblast are superimposed. Half the circumference of the normalized epiblast is flattened and fitted to its diameter (D), i.e. $\pi D/2$ is reduced to D. The primitive streak is represented by a grey stripe. The composition (to the nearest 10%) of clones contributing to amnion is shown as pie charts at the positions of clone initiation in the two upper panels. Clones not contributing to the amnion are represented by empty circles. Lower panel: composition of the clones not contributing to amniotic ectoderm in the same region as in the upper panel. Clones contributing to amniotic ectoderm are not represented for clarity. Scale bar: 50 µm. A, anterior; AVE, anterior visceral endoderm; Epi, epiblast; EPC, ectoplacental cone; EVE, embryonic visceral endoderm; ExEc, extraembryonic ectoderm; ExVE, extra-embryonic visceral endoderm; P, posterior; PAC, proamniotic canal.

The authors also received funds from the Onderzoeksraad KU Leuven (GOA/11/012).

We and the authors apologise to readers for these mistakes.

© 2018. Published by The Company of Biologists Ltd | Development (2018) 145, dev157222. doi:10.1242/dev.157222

RESEARCH ARTICLE

Amniotic ectoderm expansion in mouse occurs via distinct modes and requires SMAD5-mediated signalling

Mariya P. Dobreva[1,2,*,‡,¶], Vanesa Abon Escalona[1,2,3,‡], Kirstie A. Lawson[4,¶], Marina N. Sanchez[2], Ljuba C. Ponomarev[3], Paulo N. G. Pereira[1,2], Agata Stryjewska[5], Nathan Criem[1,2,3], Danny Huylebroeck[5], Susana M. Chuva de Sousa Lopes[6], Stein Aerts[2] and An Zwijsen[1,2,3,§,¶]

ABSTRACT

Upon gastrulation, the mammalian conceptus transforms rapidly from a simple bilayer into a multilayered embryo enveloped by its extra-embryonic membranes. Impaired development of the amnion, the innermost membrane, causes major malformations. To clarify the origin of the mouse amnion, we used single-cell labelling and clonal analysis. We identified four clone types with distinct clonal growth patterns in amniotic ectoderm. Two main types have progenitors in extreme proximal-anterior epiblast. Early descendants initiate and expand amniotic ectoderm posteriorly, while descendants of cells remaining anteriorly later expand amniotic ectoderm from its anterior side. Amniogenesis is abnormal in embryos deficient in the bone morphogenetic protein (BMP) signalling effector SMAD5, with delayed closure of the proamniotic canal, and aberrant amnion and folding morphogenesis. Transcriptomics of individual *Smad5* mutant amnions isolated before visible malformations and tetraploid chimera analysis revealed two amnion defect sets. We attribute them to impairment of progenitors of the two main cell populations in amniotic ectoderm and to compromised cuboidal-to-squamous transition of anterior amniotic ectoderm. In both cases, SMAD5 is crucial for expanding amniotic ectoderm rapidly into a stretchable squamous sheet to accommodate exocoelom expansion, axial growth and folding morphogenesis.

KEY WORDS: Amnion, Amnion fate map, BMP-SMAD, Chorion, Clonal analysis, Extra-embryonic ectoderm, Extra-embryonic–embryonic interface

INTRODUCTION

Animals classified as amniotes, including reptiles, birds and mammals, develop extra-embryonic tissues and organs that perform respiration-related, nutritional and protective functions during embryogenesis: the chorion, yolk sac, amnion and allantois. Alongside their supportive role, extra-embryonic tissues take part in the development of the early embryo proper by providing signalling cues and spatial continuity (Horn and Panfilio, 2016; Mesnard and Constam, 2010; Shao et al., 2016). The amnion is the innermost extra-embryonic tissue that delineates the fluid-filled amniotic cavity, providing space for the embryo to move freely. The amnion protects the embryo against traumas, infections and toxins (Schmidt, 1992). Despite its location at the extra-embryonic–embryonic interface, the amnion has classically not been considered a driving force in shaping the early embryo proper. However, in mice, the expansion of the amniotic cavity is crucial for the reorientation of notochord cells along the anterior-posterior axis and for the global morphogenesis of the early embryo (Imuta et al., 2014). Furthermore, in chickens the physical expansion of (pro)amnion is required for the correct positioning of the head (de Melo Bernardo and Chuva de Sousa Lopes, 2014). In humans, impaired amnion integrity, premature rupture of amnion and amniotic bands often cause preterm birth and fetal malformations, including amputations and fetal compression syndromes (Menon and Richardson, 2017; Opitz et al., 2015). Despite the importance of amnion, its developmental origin and the molecular regulation of amniogenesis remain ill-defined.

In the mouse, amnion and chorion development are intimately related. Early during gastrulation, at embryonic day (E) 6.5-7.0, extra-embryonic mesoderm emerging from the most posterior part of the primitive streak (further called 'streak') accumulates in the incipient fold at the posterior extra-embryonic–embryonic junction. This amniochorionic fold gives rise to both amnion and chorion, but initially consists only of (prechorionic) extra-embryonic ectoderm. The epiblast-derived amniotic ectoderm contributes relatively late, and only to the floor of the fold. The cuboidal chorionic ectoderm thus greatly exceeds the squamous amniotic ectoderm portion of the fold at all stages (Pereira et al., 2011). The extra-embryonic mesodermal layer, still shared by the future amnion and chorion, develops from the accumulating posterior mesoderm and lines the expanding exocoelomic cavity. When the fold is fully expanded, the chorionic walls of the proamniotic canal fuse at the extra-embryonic–embryonic junction at the embryo's anterior side, the anterior separation point (Pereira et al., 2011). This causes amnion-chorion separation, and partition of the proamniotic cavity into the amniotic, exocoelomic and ectoplacental cavities at E7.5. Shortly after amnion-chorion separation, foregut invagination begins, marking the onset of ventral folding morphogenesis. The flexible amniotic membrane envelops the entire embryo only on completion of ventrolateral morphogenesis and body wall closure (Schmidt, 1992).

Several studies indicate that bone morphogenetic protein (BMP) signalling at the extra-embryonic–embryonic interface is important for amnion-chorion separation and amnion development in the mouse (reviewed in Pereira et al., 2011). Binding of BMPs to their receptors triggers activation by phosphorylation of SMAD1,

[1]VIB-KU Leuven Center for Brain and Disease Research, Leuven 3000, Belgium. [2]Department of Human Genetics, KU Leuven, Leuven 3000, Belgium. [3]Department of Cardiovascular Sciences, KU Leuven, Leuven 3000, Belgium. [4]MRC Human Genetics Unit, MRC Institute of Genetics and Molecular Medicine, University of Edinburgh, Edinburgh EH4 2XU, UK. [5]Department of Development and Regeneration, KU Leuven, Leuven 3000, Belgium. [6]Department of Anatomy and Embryology, Leiden University Medical Center, Leiden 2333 ZC, The Netherlands. *Present address: Department of Life Sciences, Imperial College London, Silwood Park Campus, Ascot, Berkshire SL5 7PY, UK.

[‡]These authors contributed equally to this work
[§]Lead contact

[¶]Authors for correspondence (m.dobreva@imperial.ac.uk; kirstie.lawson@igmm.ed.ac.uk; an.zwijsen@kuleuven.be)

A.Z., 0000-0002-8583-1721

Received 19 July 2017; Accepted 30 May 2018

Development (2018) 145, dev157222. doi:10.1242/dev.157222

SMAD5 and SMAD9, which co-regulate BMP-responsive gene expression (Katagiri and Watabe, 2016). SMAD5-deficient embryos develop severe morphogenesis defects (Chang et al., 1999; Yang et al., 1999), amnion-chorion separation is delayed and the anterior separation point is shifted posteriorly (Bosman et al., 2006). After closure of the proamniotic canal, a striking aggregate of cells develops anteriorly in the amnion (Chang et al., 1999). These aggregates ectopically express the mesoderm inducer *Nodal*, in addition to *T*, *Fgf8* and *Eomes*, all established streak mesoderm markers (Pereira et al., 2012). The aggregates are variable in size, position and relative composition at E8.5-E9.0. In contrast to the avascular wild-type (WT) amnion, the aggregates become vascularized and develop red blood cells and primordial germ cell (PGC)-like cells (Bosman et al., 2006; Chang et al., 1999), all posterior streak derivatives. BMP-SMAD signalling is active during amniogenesis as shown in a *BRE::LacZ* reporter mouse that monitors transcriptional activity of phosphorylated BMP-SMAD proteins (Cajal et al., 2014; Dobreva et al., 2012). Reporter activity is present in the amniotic ectoderm component of the amniochorionic fold, the separated amnion, the anterior midline region distal to the extra-embryonic/embryonic junction and, from amnion-chorion separation onwards, in the lateral junctions of amnion with surface ectoderm. In other species, BMP-SMAD signalling is also crucial for amnion-like tissue development, e.g. in amniogenesis in human pluripotent stem cell cultures (Shao et al., 2016), and in defining amnion and serosa or amnioserosa in different insect species (Rafiqi et al., 2012; Horn and Panfilio, 2016). Furthermore, prominent amniotic expression of *BMP4* has been reported in cynomolgus monkeys (Sasaki et al., 2016).

Little is known about the developmental origin of the amnion, particularly the amniotic ectoderm (Kinder et al., 2001; Lawson et al., 1991). To remedy this, we made a prospective lineage analysis by labelling single epiblast cells (Lawson et al., 1991) in the proximal half of WT mouse embryos before and early in gastrulation (E6.2-E6.5). We identified four distinct types of clonal growth pattern that expand amniotic ectoderm differently and with different magnitude. Additionally, we investigated the earliest steps of abnormal amniogenesis in mice deficient in SMAD5 by sequencing the mRNA (RNA-seq) of individual control and mutant amnion samples, and by chimera analysis. Correlating these data with the clonal analysis supports the conclusion that the impaired amniogenesis in *Smad5* mutants results from the two main cell populations in amniotic ectoderm being affected by the SMAD5 deficiency.

RESULTS

Amniotic ectoderm is derived from the proximal-anterior and anterolateral epiblast

To gain insight into the location of amnion progenitors and to trace their contribution in amniotic ectoderm, we labelled single epiblast cells in the proximal half of WT embryos at prestreak (PS) and early-streak (ES) stages and analysed the resulting clones. Two properties of single-cell labelling followed by short-term retrospective lineage analysis were exploited in this approach. First, labelling by iontophoretic injection enables analysis of clones with known spatial and temporal origins. It gives fine-resolution fate maps and the opportunity to reconstruct morphogenetic change from patterns of clonal expansion during a period of rapid growth. Second, lineage analysis of prospectively labelled clones allows the clonal history to be inferred within the cell layer of origin. Thus, the time trajectory within the amniotic ectoderm, which is continuous with the epiblast within which the clone arose, can be traced with confidence retrospectively.

The fate maps of PS and ES stages show that the amniotic ectoderm is derived mainly from mixed fate progenitors in the proximal anterior and anterolateral epiblast, whereas amniotic mesoderm progenitors, also of mixed fate, lie more posteriorly and distally. These findings are graphically displayed in Fig. 1. From the

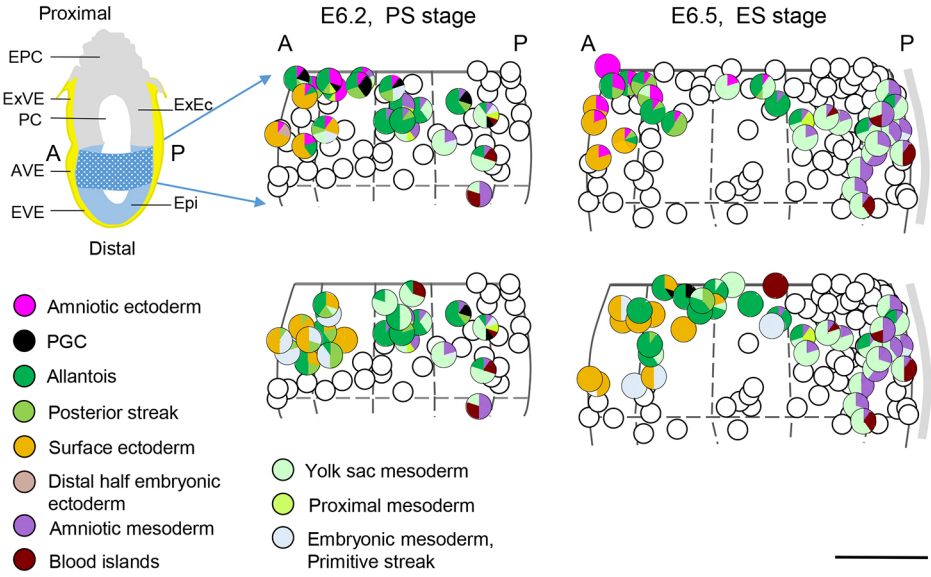

Fig. 1. Amnion fate map. Fate maps of amniotic ectoderm and amniotic mesoderm. Top left: cartoon of a midsagittal section of an E6.2, prestreak stage (PS) embryo. The proximal half of the epiblast cup (blue pattern) is expanded in the right panels and projected on the sagittal midline of PS and early-streak (ES) stages. Left and right halves of the epiblast are superimposed. Half the circumference of the normalized epiblast is flattened and fitted to its diameter (D), i.e. πD/2 is reduced to D. The primitive streak is represented by a grey stripe. The composition (to the nearest 10%) of clones contributing to amnion is shown as pie charts at the positions of clone initiation in the two upper panels. Clones not contributing to the amnion are represented by empty circles. Lower panel: composition of the clones not contributing to amniotic ectoderm in the same region as in the upper panel. Clones contributing to amniotic ectoderm are not represented for clarity. Scale bar: 50 µm. A, anterior; AVE, anterior visceral endoderm; Epi, epiblast; EPC, ectoplacental cone; EVE, embryonic visceral endoderm; ExEc, extra-embryonic ectoderm; ExVE, extra-embryonic visceral endoderm; P, posterior; PC, proamniotic cavity.

Development (2018) 145, dev157222. doi:10.1242/dev.157222

triangular-shaped region spanning the anterior midline that generated amniotic ectoderm, only a minority of labelled descendants (8%, 245/3032 from 61 clones) were in amniotic ectoderm. Not all epiblast cells in this region gave rise to amniotic ectoderm, but the composition of the clones was otherwise indistinguishable from that of their amnion-contributing neighbours. This showed an anterior-posterior transition in the fate map from predominantly surface ectoderm to extra-embryonic mesoderm (Fig. 1, comparing upper and lower panels). The amniotic ectoderm therefore develops from a relatively small number of descendants of proximal-anterior and anterolateral epiblast that, before and at the onset of gastrulation, is mainly prospective surface ectoderm and extra-embryonic mesoderm.

Amniotic ectoderm is established via several routes

The detailed findings from the 28 clones that contributed to amniotic ectoderm are presented in Fig. 2, Table 1 and Fig. S1. Overall, four clone types were distinguished on the basis of their distribution within the amniotic ectoderm (Fig. 2) and clone composition (Table 1).

Type I clones originated in a very restricted region of extreme proximal anterior/anterolateral epiblast, abutting the extra-embryonic ectoderm: they were mixed clones with descendants mainly in extra-embryonic structures, posterior streak and PGCs (Table 1). Type I clones were found at PS , but not at ES, stage (see Fig. S2 for possible explanations). These clones spread in the amniotic ectoderm from the anterior separation point to the posterior edge of the amnion, indicating that they contributed to the amnion from its inception: the position of the most anterior cells of these clones reflected the origin of the progenitors in association with presumptive chorionic ectoderm. The first amniotic cell of the clone would have been an extreme posterior (proximal) epiblast or posterior streak cell in contact with the floor of the early amniochorionic fold; it then divided, leaving one daughter associated with the prechorionic ectoderm, the other with the epiblast/streak. Succeeding divisions expanded the amniotic portion of the fold. Clones #1 and #2 must have gone through two cell generations in the epiblast before contributing one cell (clone #1), or one followed by two (clone #2), to the emergent amnion between E6.8 and E7.1 (Fig. S1A) at midstreak (MS) to late-streak (LS) stages [see Fig. 3.5 of Lawson and Wilson (2015) for correlation of age and stage]. Subsequently, the clones expanded through the following three or two generations, respectively (Fig. S1A). The distribution pattern of Type I clones indicates that these clones

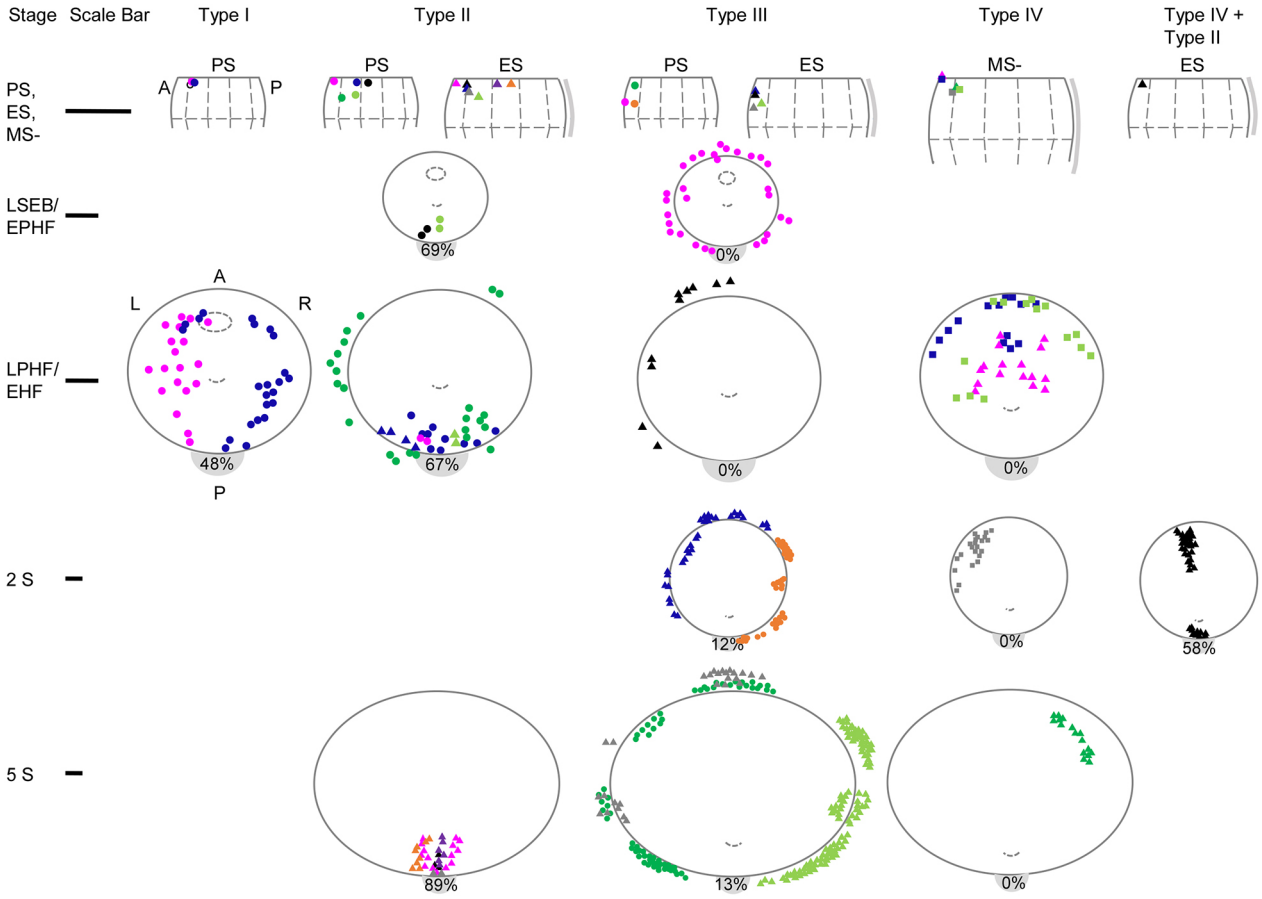

Fig. 2. Spread of clone descendants in amniotic ectoderm. Clonal spread in amniotic ectoderm and associated surface ectoderm. Each clone within a type is identified by a colour/shape combination (Table 1). Top row: the positions of clone progenitors are plotted, as in Fig. 1, on scaled representations of the proximal half of the epiblast at different initial stages (PS, ES and MS-). Scale bars: 100 µm. The top edge of the diagram is at the junction with the apposing extra-embryonic (prechorionic) ectoderm. The position of the progenitor of the unplotted Type I PS clone #3 is shown as an empty circle. Lower rows: the view of clone distribution in the amniotic ectoderm (solid line ellipses) is from dorsal with anterior (A) at the top. The projected positions of the closing/closed proamniotic canal and node are indicated by an ellipse (dashed line) and an arc (dashed line), respectively. Cells plotted outside the amnion are in the adjacent non-neural ectoderm (mainly surface ectoderm). The number in the grey crescent at the posterior edge of the amnion is the total number of extra-embryonic mesoderm and posterior streak cells in the clones expressed as a percentage of the total labelled cells in the embryos contributing to the plot. Clones #2 (Type I, dark blue), #17 (Type III, dark blue) and #27 (Type IV, light green) are shown in LR mirror image to reduce overlapping in display.

Table 1. Record of clones contributing to amniotic ectoderm (see also Table S6)

									Clone distribution							
Type	Clone	Colour code/ shape[1]	Initial stage[2]	Final stage[2]	Nominal age [E[3] days] at labelling	Clone age (h)	Clone size	Cdt[4] (h)	Amniotic ectoderm	Amniotic meso-derm	Posterior streak	Allantois	Yolk sac meso-derm	PGC[5]	Surface ectoderm	Rest of embryo
Type I	1	Magenta/C	PS	LPHF/EHF	6.05	45	67	7.42	19 (28%)	0	8 (12%)	32 (48%)	0	3 (5%)	0	5[6] (7%)
	2	Dark blue/C	PS	EHF	6.19	41	31	8.28	23 (74%)	0	0	5 (16%)	0	0	0	3[6] (10%)
	3	[unplotted] [7]	PS+	3/4S	6.27	42.5	52	7.46	16 (31%)	0	12 (23%)	24 (46%)	0	0	0	0
Type II	4	Magenta/C	PS	EPHF	6.27	42.5	62	8.58 [2]	2 (3%)	0	8 (13%)	38 (63%)	3 (5%)	10 (16%)	0	0
	5	Dark blue/C	PS−	EPHF	6.21	42	69	6.9	9 (13%)	5 (7%)	0	45 (65%)	6 (9%)	0	0	4[6] (6%)
	6	Black/C	PS−	LSEB	6.12	44	84	6.88	2 (2%)	0	22[8] (26%)	30 (36%)	8 (10%)	4 (5%)	0	18[8,9] (21%)
	7	Green/C	PS−	LPHF	6.18	39	∼150	∼6.26 [2]	7 (4%)	1 (0.6%)	6 (4%)	26 (17%)	36 (23%)	0	18 (15%)	56[8,9] (36%)
	8	Light green/C	PS−	LSEB	6.29	40.5	18	9.71	2 (11%)	0	6 (33%)	4 (23%)	0	6 (33%)	0	0
	9	Magenta/T	ES	4/5S	6.69	40	43	7.37	15 (35%)	0	7 (16%)	21 (49%)	0	0	0	0
	10	Black/T	ES	6S	6.64	40.5	40	7.61	3 (8%)	0	∼30 (75%)	∼7 (17%)	0	0	0	0
	11	Purple/T	ES	6S	6.54	42	39	7.95	6 (15%)	0	0	0	33 (85%)	0	0	0
	12	Orange/T	ES−	5/6S	6.69	40	95	6.09	8 (8%)	0	9 (10%)	40 (42%)	38 (40%)	0	0	0
	13	Dark blue/T	ES+	EPHF/LPHF	6.55	19.75	11	5.71	4 (36%)	0	5 (46%)	0	2 (18%)	0	0	0
	14	Grey/T	ES	5S	6.59	41	∼100	∼7.26 [2]	2 (2%)	0	13 (13%)	85 (85%)	0	0	0	0
	15	Light green/T	ES	LPHF	6.71	22.5	18	5.4	2 (11%)	0	9 (50%)	7 (39%)	0	0	0	0
Type III	16	Magenta/C	PS	LSEB	6.65	24.5	35	5.93 [2]	5 (14%)	0	0	0	0	0	24 (69%)	6[10] (17%)
	17	Dark blue/T	ES+	3S	6.5	40	31	8.07	8 (26%)	0	0	0	0	0	23 (74%)	0
	18	Black/T	ES−	(L)PHF	6.85	21	10	6.32	2 (20%)	0	0	0	0	0	8 (80%)	0
	19	Grey/T	ES+	6/7S	6.88	37.5	27	7.89	5 (19%)	0	0	0	0	0	22[11] (81%)	0
	20	Green/C	PS/ES−	7S	6.57	41.5	73	6.7	10 (14%)	0	0	6 (8%)	0	0	57 (78%)	0
	21	Light green/T	ES	6S	6.48	42.75	∼250	∼6.14 [2]	14 (6%)	0	∼27 (11%)	12 (5%)	0	0	∼197 (78%)	0
	22	Orange/C	PS	LHF	6.67	40.5	44	7.42	8 (20%)	0	0	9 (20%)	0	0	27 (60%)	0
Type IV	23	Magenta/T	ES+	EHF	6.57	24.5	16	6.06	16 (100%)	0	0	0	0	0	0	0
	24	Dark blue/S	MS−	LPHF	6.67	20.25	14	5.32	14 (100%)	0	0	0	0	0	0	0
	25	Grey/S	MS	LHF	6.54	19.25	22	5.56 [2]	22 (100%)	0	0	0	0	0	0	0
	26	Green/T	ES+	5S	6.84	36	16	9	16 (100%)	0	0	0	0	0	0	0
	27	Light green/S	MS	LPHF	6.57	23	14	6.04	14 (100%)	0	0	0	0	0	0	0
Type IV+II	28	Black/T	ES−	3S	6.59	41	90	6.32	38 (42%)	0	10 (11%)	42 (47%)	0	0	0	0

[1]Used in Fig. 2: C, circle; S, square; T, triangle; [2]stage terminology as in Lawson and Wilson (2015); [3]E, embryonic day (see Materials and Methods for details); [4]clone doubling time (Cdt) extracted from Fig. S1 {[2] refers to two sibling progenitors; this affects the calculation of the Cdt}; [5] PGC contribution of clones 1, 3, 5 and 7 was summarized in Lawson and Hage (1994); [6]proximal mesoderm; [7] insufficient spatial detail recorded for plotting; [8]posterior half of the streak; [9]lateral plate mesoderm; [10]distal half of the epiblast; [11]three buccal, two oral plate, 11 ventral ectoderm of the prosencephalon (Cajal et al., 2012), two surface ectoderm at midbrain-hindbrain boundary, four surface ectoderm at S4.

Development (2018) 145, dev157222. doi:10.1242/dev.157222

Development (2018) 145, dev157222. doi:10.1242/dev.157222

represent the founding population of the amniotic ectoderm until amnion closure.

Type II clones originated over a larger area of proximal-anterior epiblast than Type I. These mixed clones contributed mainly to extra-embryonic mesoderm, posterior streak and PGCs with generally only a small minority of descendants in amniotic ectoderm (Table 1). The contribution was limited to posterior amnion (Fig. 2), and was slightly later than Type I and over a longer period (E7.2-E8.1) (Fig. S1B). Hence, Type II descendants moved into the established primordium and remained as short files that had not extended further than 15% of the anterior-posterior length of the amnion by early somite stages (Fig. 2). At the LS stage, the amnion ectoderm consists of only about 20 cells [EMA10 eMouseAtlas (Armit et al., 2017)] and, given the behaviour of Type II clones, the founding population associated with the chorionic ectoderm is probably complete by this time. Therefore, the founding population of the amniotic ectoderm appears to be both small and established within a narrow time window.

Type III clones originated in the proximal quadrant of epiblast spanning the anterior midline i.e. in prospective surface ectoderm, which was the main clonal component. Single, small inclusions of labelled cells in the periphery of the amnion were found between the axial level of the midbrain and the node (Fig. 2). The size of the inclusion expanded with the rest of the clone. The inferred clonal histories (Fig. S1C) indicate that the inclusion of two cells would have occurred between E7.3 and E7.7 [expected early preheadfold (EPHF) to late headfold (LHF)], i.e. in the period of rapid amnion expansion during and after closure, onset of axial elongation from the node, expansion of the neural folds and initiation of the foregut. This suggests that inclusion into the periphery of the amnion from embryonic ectoderm is usually limited to a period when considerable adjustments to turgor in the amniotic and yolk sac cavities occur, and when the rostral half of the embryo is growing rapidly.

Type IV clones originated in extreme proximal anterior to anterolateral epiblast, spanning the midline. They were generated between ES+ and MS stages within the same area as the earlier Type I clones, but were exceptional in being lineage restricted with all descendants in amniotic ectoderm (Table 1, Fig. 2). The pattern of clonal spread at late prehead fold (LPHF)/early headfold (EHF) indicated that early descendants entered the amnion at, or close to, the anterior midline. They not only expanded the amniotic ectoderm anterior to the anterior separation point, but also contributed to the main body of amniotic ectoderm laid down by the original Type I founding population (Fig. 3A,B). Descendants in somite-stage embryos were found concentrated mainly between the axial levels of heart and hindbrain.

An interesting mixed type clone (#28) contributed to the amnion from both anterior and posterior. The inferred history (Fig. S1D) indicated that the ES progenitor would have divided twice before one cell became restricted to amniotic ectoderm (behaving further as Type IV), and the remaining three cells behaved as Type II, contributing further descendants to posterior amnion, posterior streak and allantois. Together, these results indicate that extreme proximal descendants of PS- or ES-stage epiblast that remain anterior become part of a relatively late population of exclusively amniotic ectoderm precursors that expand the amnion specifically from the anterior.

In brief, Type I descendants initiate amniotic ectoderm. Until closure of the proamniotic canal, Type I and II descendants, both from mixed fate progenitors, expand the amniotic ectoderm. Around the time of proamniotic canal closure and after amnion-chorion separation, the amniotic ectoderm becomes extensively expanded directly from the anterior by the late-contributing, lineage-restricted Type IV descendants. Type III descendants expand the amnion only at the periphery. The behaviour and timing of the different groups that constitute the amniotic ectoderm are summarized in Figs 3B and 8A,B.

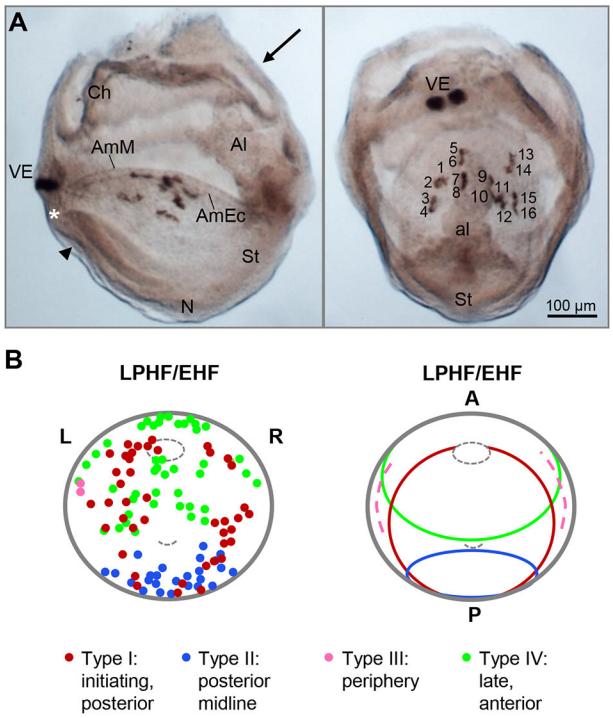

Fig. 3. Illustration and summary of amniotic ectoderm clones. (A) Lateral view, anterior facing left, and posteriodorsal view (indicated by arrow in lateral view) of a mouse embryo with HRP-labelled Type IV clone (#23) in the amniotic ectoderm (Table 1, Fig. 2). The clone was initiated close to the midline at the extra-embryonic–embryonic junction (Fig. 2), as indicated by the VE marker clone. As the epiblast clone is a pure clone, there is no supporting evidence about the time of entry of descendants into the amniotic ectoderm. The pattern of four files of four cells [(1-4)(5-8)(9-12)(13-16)] oriented anterior-posteriorly indicates that the progenitor divided twice before all four descendants left the periphery of the amniotic ectoderm during the same cell cycle and went through two additional cycles of oriented cell division. Two other Type IV clones (#24 and #27) indicate that cells may divide once or twice at the anterior periphery while releasing descendants to start populating the anterior amniotic ectoderm. The asterisk and arrowhead mark the amniotic ectoderm/embryonic ectoderm junction and the incipient foregut pocket, respectively. Scale bar: 100 µm. (B) Combined distribution (left) of the four types of amniotic ectoderm clones (Fig. 2) in an LPHF/EHF amnion, and simplified territories (right). Anterior (A) to the top. The projected positions of the closed PAC and node are indicated by a small ellipse and arc (dashed lines), respectively. Type I descendants initiate the primordium and establish the amniotic ectoderm posterior to the anterior separation point, whereas Type II descendants populate the most posterior midline subregion. The lineage-restricted Type IV descendants produce amniotic ectoderm anterior to the ASP, and also contribute to the already established Type I territory. Type III descendants expand the amnion only at the periphery. Al, allantois; AmEc, amniotic ectoderm; AmM, amniotic mesoderm; Ch, chorion; N, node; St, streak; PAC, proamniotic canal; VE, visceral endoderm.

The amnion of *Smad5* mutants expresses two transcriptionally distinct signatures

In normal early somite-stage mouse conceptuses, amnion appears as a translucent and stretched tissue. In contrast, most *Smad5* knockouts (KOs) are distinguished by the presence of a variable aggregate of cells in the amnion. Additionally, mutants have various

Development (2018) 145, dev157222. doi:10.1242/dev.157222

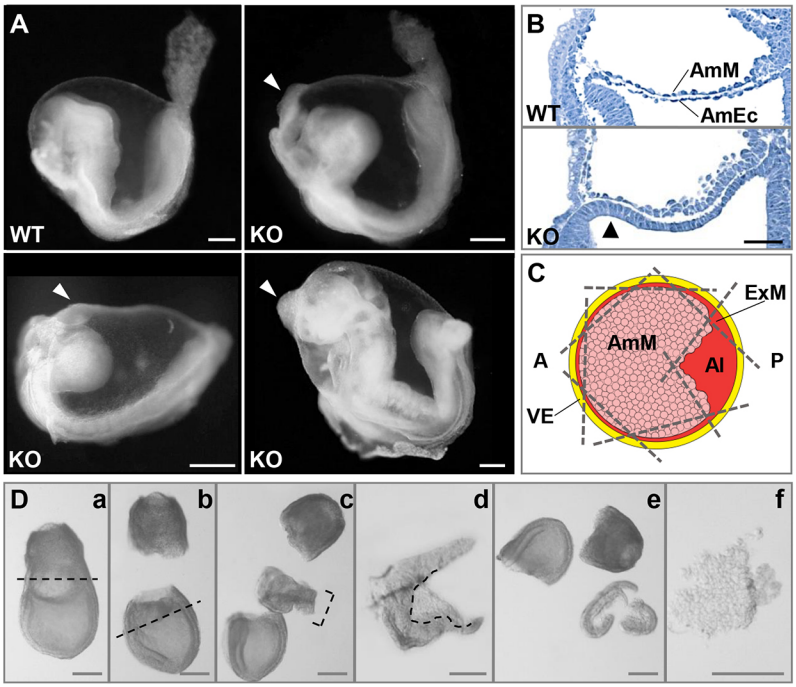

Fig. 4. Phenotype of *Smad5* mutants and amnion microdissection procedure. (A) Appearance of early somite stage wild-type (WT) and *Smad5* knockout (KO) embryos. The mutant amnion contains an anteriorly localized tissue aggregate (arrowhead). Scale bars: 200 µm. (B) Longitudinal sections of E7.5 LPHF-stage WT and *Smad5* KO embryos stained with Haematoxylin. Amniotic ectoderm (AmEc) is thickened in mutants (arrowhead). Scale bar: 50 µm. AmM, amniotic mesoderm. (C) Scheme of a dorsal view of an amnion positioned to trim it free (see D) from neighbouring tissues; broken lines represent cuts. Al, allantoic bud; AmM, amniotic mesoderm; ExM, extra-embryonic mesoderm; VE, visceral endoderm. Anterior to the left. (D) Amnion microdissection procedure for an E7.5 LPHF embryo. Following removal of the proximal (a) and distal (b) parts of the conceptus (cuts at the broken lines), the extra-embryonic–embryonic junction region (bracket in c) is flipped 90° and the borders and allantoic bud are trimmed from the amniotic tissue (d). The remainder of the conceptus (e) and the isolated amniotic tissue (f) are used for genotyping and transcriptome analysis, respectively. Scale bars: 200 µm.

ventral folding defects (Chang et al., 1999) (Fig. 4A). Amniotic ectoderm is cuboidal before aggregate formation, in contrast to the squamous control amnion, and the junction between amniotic and embryonic ectoderm is anteriorly less pronounced in all *Smad5* mutants (Fig. 4B).

We investigated the molecular differences between WT and *Smad5* mutant amnion by RNA-seq analysis. Amnions were microdissected (Fig. 4C,D) from control (n=6), and stage-matched littermate *Smad5* knockout (n=6) embryos ranging between EPHF and three-somite (3S) stages (Table S1), before major morphological differences become apparent. We synthesized and amplified cDNA from individual amnion samples. Absence of contamination with surrounding tissues was confirmed by quantitative reverse-transcription PCR (RT-qPCR) marker analysis in control samples (Fig. S3A).

The variance-normalized counts of the RNA-seq data (Table S1) were used for expression visualization, clustering and differential gene expression analysis. Unsupervised clustering of all 12 samples by principal component analysis (PCA) resulted in clustering of five of six control samples and the segregation of the six knockout samples into two distinct groups, which we named KO-SetA and KO-SetB (Fig. 5A). Ctrl6.1 was determined to be an outlier and omitted from further analysis. Gene set enrichment analysis (GSEA) of the top differentially expressed genes (adjusted P-value <0.05) showed that KO-SetA samples were significantly enriched for categories such as ‘gastrulation’, ‘mesoderm development’ and ‘cell fate specification’, whereas gene sets like ‘integrin binding’ and ‘regulation of cell adhesion’ were under-represented (Fig. S3B,C, Table S2, Supplementary Materials and Methods). Conversely, KO-SetB samples were enriched in categories such as ‘placenta development’ and ‘extra-embryonic ectoderm’, whereas ‘extracellular matrix’ and ‘epithelial-to-mesenchymal transition (EMT)’ sets were downregulated.

Closer examination of samples with the KO-SetA signature (Fig. 5B,C, Tables S3 and S4) confirmed and expanded our former *in situ* hybridization results on ectopic expression of *Nodal*, *T*, *Lefty2*, *Wnt3* and *Fgf8* in *Smad5* mutant amnion (Pereira et al., 2012). Furthermore, KO-SetA samples significantly overexpressed several markers related to EMT, streak and streak-derived mesoderm (Fig. 5B,C, Table S3). They include the streak mesoderm-related *Fst* (57-fold increase in KO-SetA compared with control), *Zic3* (79-fold); the Nodal co-receptor *Tdgf1* or *Cripto* (22-fold); and the Nodal target genes *Fgf5* (71-fold), *Mixl1* (14-fold) and *Mesp1* (18-fold). Remarkably, several extra-embryonic ectoderm markers were robustly enriched in samples with KO-SetB signature (Fig. 5B,C, Tables S3 and S4). These included genes such as *Elf5* (391-fold more in KO-SetB compared with control), *Esrrb* (202-fold), *Sox2* (15-fold), *Sox21* (107-fold) and *Cldn3* (146-fold).

The two KO sets shared some features. Under-representation of genes encoding ECM components, such as collagens, and downregulation of amnion-enriched transcripts like *Postn* (Dobreva et al., 2012), *Tfap2a* and *Twist1* (Bosman et al., 2006) and *Flrt3* (Egea et al., 2008), suggested loss of amnion identity (Fig. 5C, Fig. S3B,C, Table S3 and S4). *Eomes* – a streak marker and target gene of Nodal signalling (Arnold et al., 2008), and also a marker for extra-embryonic ectoderm (Ciruna and Rossant, 1999) – was found enriched in both KO sets. Target genes of BMP signalling, such as *Smoc2*, *Postn* (Inai et al., 2008) and *Flrt3* (Tomás et al., 2011), were under-represented in both KO sets (Table S3); however, differential expression of other target genes of BMP/SMAD5, BMP ligands and modulators of BMP signalling were specifically observed in KO-SetB samples, e.g. *Msx1*, *Hand1* and noggin (*Nog*).

The distribution of KO-SetA and KO-SetB expression profiles was validated by RT-qPCR in a larger cohort of 25 E7.5 littermate control-knockout amnion sample pairs. We selected four KO-SetA (*Fgf5*, *Nodal*, *T* and *Lefty2*) and four KO-SetB (*Elf5*, *Essrb*, *Cldn4* and *Sox2*) genes enriched in one but not the other set (Fig. 5C, Table S5). One of 25 pairs showed differential expression of only one of the selected markers, and was therefore not categorized. The majority of the pairs (64%) segregated either into a KO-SetA (48%) or KO-SetB (16%) signature (Fig. 5D). Several pairs (32%) showed an intermediate signature with two or more markers (over)expressed

Development (2018) 145, dev157222. doi:10.1242/dev.157222

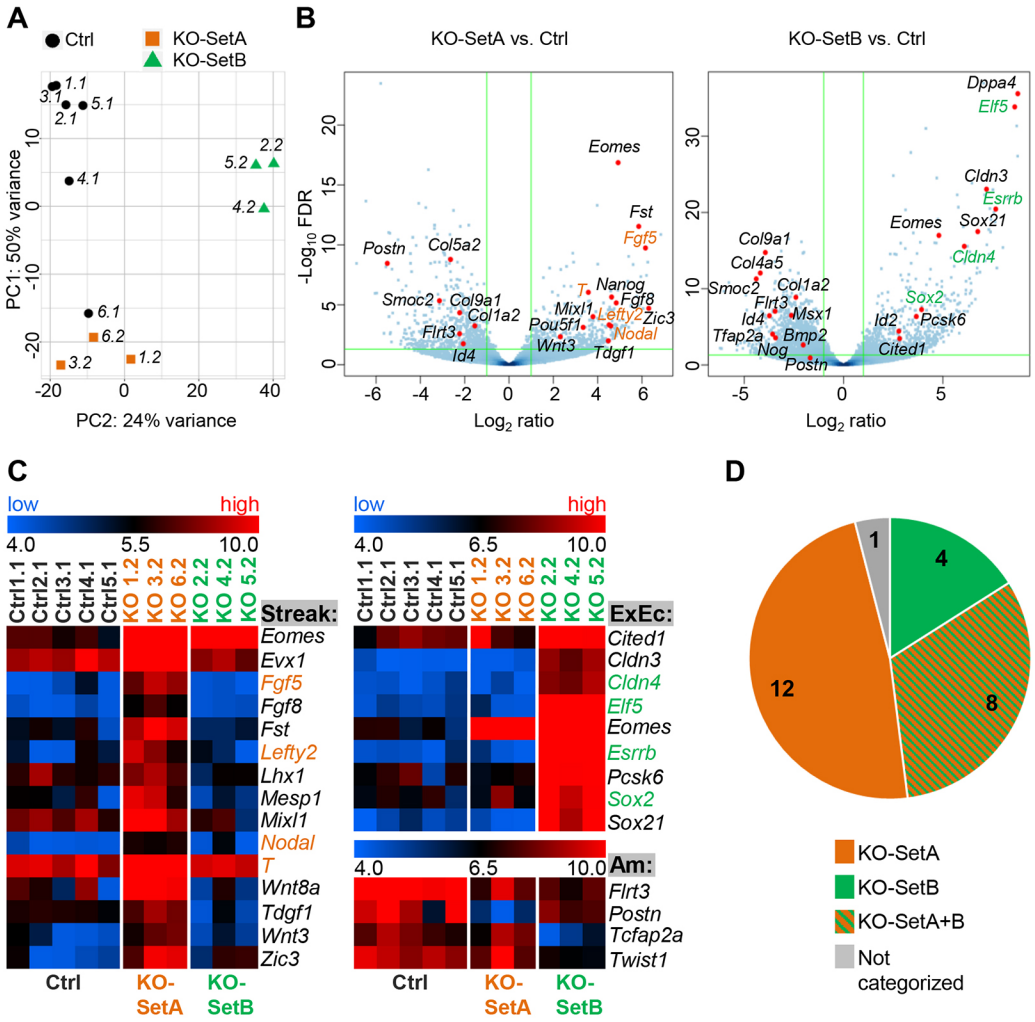

Fig. 5. Differential expression analysis shows two sets of mutants with distinct signatures. (A) Clustering of control (Ctrl) and *Smad5* mutant (KO) amnion samples (details on identity tags of samples are provided in Table S1) by principal component analysis (PCA). The KO samples robustly segregated into two distinct groups. (B) Volcano plots showing the DESeq2-estimated log2-ratios versus the significance as the negative log10 adjusted *P*-value (FDR). Green lines correspond to the used thresholds on the FDR (<0.05) and on the log fold change (<−1 and >1). (C) Expression heat maps for selected transcripts. The scale indicates variance-stabilized values from minimum to maximum limits of expression values. The mid-values represent the median. Streak/mesoderm markers are enriched in KO-SetA, and extra-embryonic ectoderm markers (ExEc) are enriched in KO-SetB. (D) Independent validation of RNA-seq findings. Distribution of mutant expression signatures among 25 littermate knockout/control pair amnion samples based on RT-qPCR for the KO-SetA markers *Nodal*, *Lefty2*, *T* and *Fgf5* (orange) and KO-SetB markers *Cldn4*, *Elf5*, *Esrrb* and *Sox2* (green). A knockout was considered to belong to a particular set if it overexpressed (>3-fold) at least two of the set markers and not more than one marker of the other set. Knockouts with mixed signature (KO-SetA+KO-SetB) overexpressed two or more markers of each set. Noncategorized samples are in grey.

from each set. Collectively, the data demonstrate the presence of two transcriptionally distinct signatures in the amnion of *Smad5* mutants. The high prevalence of the intermediate signature suggests transition from a KO-SetB to a KO-SetA category (progressive loss of ExEc inclusion features because of ExEc transdifferentiation into an aggregate), or co-existence of mixed KO-SetA and KO-SetB phenotypes.

Fgf5 and Elf5, KO-SetA and KO-SetB markers, are ectopically localized in mutant amniotic ectoderm

Subsequently, we documented where the top overexpressed markers of KO-SetA and KO-SetB localize in mutant amnion. Ectopic *T*, *Nodal* and *Wnt3* expression, and Nodal- and β-catenin-mediated signalling in amniotic ectoderm of *Smad5* mutants was previously documented (Pereira et al., 2012). Here, we show the expression of a new SetA marker, *Fgf5*. *Fgf5* is normally expressed in the epiblast at ES stage, including in the region in which amniotic ectoderm precursors reside. Its expression is lost anteriorly in the late streak early allantoic bud (LSEB) and *Fgf5* is absent in normal amnion (Li et al., 2013). We found *Fgf5* expressed ectopically in nine of ten *Smad5* EPHF-EHF embryos. The ectopic expression was prevalent in the anterior embryonic ectoderm and continuous with the anterior amniotic ectoderm, consistent with the continuous cuboidal ectoderm shown in Fig. 4B. Its range of extension into amniotic ectoderm was variable, but could reach as far posteriorly as the abnormally positioned anterior separation point (Fig. 6A).

Next, we assessed the localization of a KO-SetB marker, Elf5, an extra-embryonic ectoderm-specific transcription factor (Donnison et al., 2005) and Oct4/Pou5f1, normally detected in amniotic ectoderm at EPHF stages (Downs, 2008). In E7.5 control embryos, amniotic ectoderm was $Oct4^{+}$ and $Elf5^{-}$, while extra-embryonic ectoderm showed Elf5 presence but no Oct4 (Fig. 6B, Ctrl). This

Development (2018) 145, dev157222. doi:10.1242/dev.157222

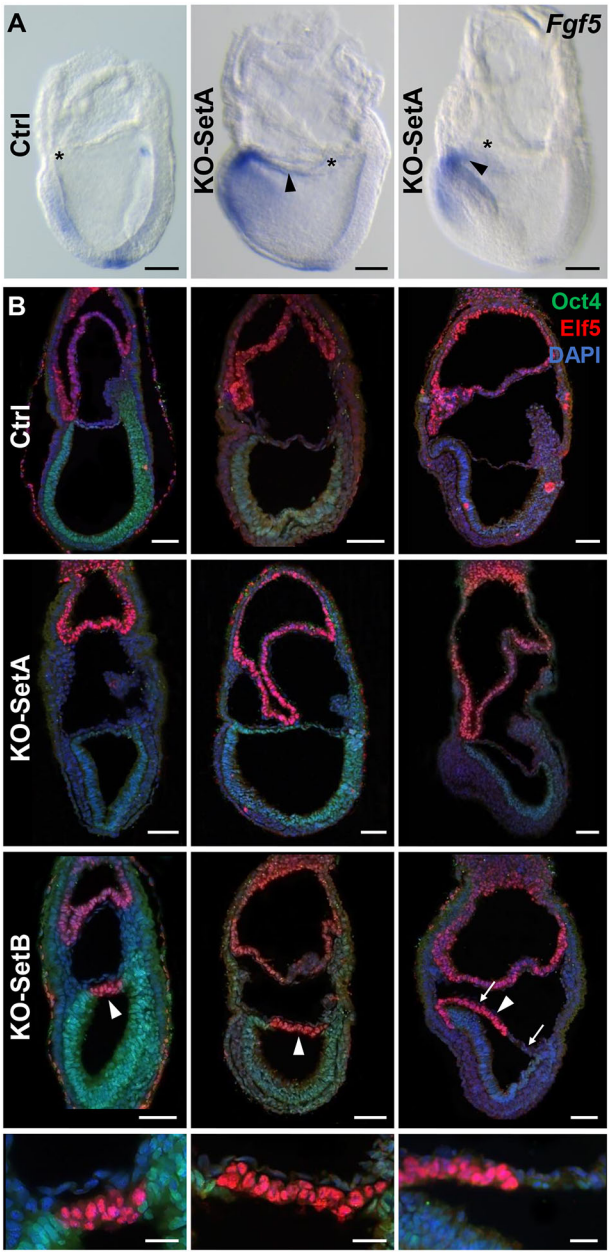

Fig. 6. Ectopic presence of the epiblast marker *Fgf5* and the extra-embryonic marker Elf5 in the mutant amnion. (A) *In situ* hybridization of control (EPHF) and two *Smad5* knockout (EHF) embryos for *Fgf5*, a KO-SetA-enriched transcript. The *Fgf5*$^{+}$ segment had a variable extension in the mutant amniotic ectoderm (KO-SetB embryos, arrowheads). The anterior separation point (ASP, asterisks), where the proamniotic canal closes and amnion and chorion separate, shifted posteriorly in mutants. Scale bars: 100 µm. (B) Longitudinal sections of control and *Smad5* knockout embryos stained with anti-Oct4/Pou5f1 and anti-Elf5 antibodies. Oct4 is present in amnion and Elf5 in chorion in control embryos and in 80% of *Smad5* knockout embryos (KO-SetA embryos), while 20% of the mutants have an Oct4^{-}, Elf5^{+} segment in the amnion (KO-SetB embryos, arrowheads). Magnifications of these areas are shown. The magnified region in the lower right embryo is bracketed by arrows. Scale bars: 75 µm; 25 µm in magnifications.

pattern was present in the majority of the mutants (20/25) (Fig. 6B, KO-SetA). However, in a fraction of the mutants (5/25), a portion of ectoderm, continuous with the amniotic ectoderm, was strongly Elf5^{+} and Oct4^{-} (Fig. 6B, KO-SetB). This pattern did not correlate with a specific developmental stage (data not shown). The ectopic presence of Elf5, but also of Eomes (Fig. S4), in amniotic ectoderm in some mutants is suggestive of inclusion of extra-embryonic ectoderm, although *de novo* transcript induction could not be excluded at this stage.

Tetraploid chimeras support aberrant expansion of amniotic ectoderm in *Smad5* mutants

Based on (1) the delayed closure of the proamniotic canal and amnion-chorion separation in *Smad5* knockout embryos (Fig. 6); (2) the two different KO set signatures (Fig. 5); and (3) the robust expression of extra-embryonic ectoderm enriched transcripts in the KO-SetB samples (Fig. 5), we reasoned that a deficit in the amniotic ectoderm could result in compensatory inclusion of nonamniotic epiblast tissue and/or trailing extra-embryonic ectoderm into the mutant amnion.

Tetraploid (4n) complementation assays were performed to determine whether an extra-embryonic ectoderm inclusion occurs in the mutant amnion, and whether such inclusions transdifferentiate into aggregates (Fig. 7A). Donor embryonic stem cells (ESCs) in ESC↔4n embryo chimeras normally give rise to all epiblast-derived tissues, including the extra-embryonic mesoderm and amniotic ectoderm. Conversely, tetraploid descendants are restricted to trophectoderm derivatives, including chorionic extra-embryonic ectoderm and extra-embryonic endoderm lineages. The segregation of descendants of ESCs and tetraploid cells in a chimera thus enables a distinction to be made between cells of epiblast or extra-embryonic ectoderm origin. GFP^{+} WT and *Smad5* knockout ESCs (Bosman et al., 2006) were aggregated with GFP^{-} tetraploid embryos (Fig. 7A).

Amniotic ectoderm and amniotic mesoderm were indeed GFP^{+} in control chimeras (*WT;GFP*$^{+}$ ESC↔4n WT) (Fig. 7B, Fig. S5A). The majority of the knockout chimeras (Table 2) had uniformly GFP^{+} amniotic ectoderm, like the other epiblast-derived tissues. In most of the E7.5 knockouts (16/21), much of the amniotic ectoderm was morphologically indistinct from the anterior embryonic ectoderm (Fig. 7C,D, Fig. S5B). Many of these embryos (Table 2) displayed a 'head-out' phenotype, with the anterior epiblast/future head region protruding outside the visceral yolk sac (Fig. 7C, Fig. S5E) as if anterior amniotic ectoderm was lacking. In a few KO chimeras (3/35, 9%) the GFP^{+} SMAD5-deficient posterior amniotic ectoderm appeared undersized and stretches of tetraploid (GFP^{-}) extra-embryonic ectoderm were trapped in the amnion (Fig. 7E, Fig. S5G-H).

While nearly all conventional *Smad5* knockout embryos develop an anterior aggregate in the amnion beyond the four-somite stage (Pereira et al., 2012), only 1/14 E8.5 knockout chimeras had an anterior aggregate (Fig. 7D). A more posterior thickening was observed in 5/14 knockout chimeras (Fig. S5C,F). Amniotic aggregates were always GFP^{+}, confirming their embryonic origin. Therefore, Elf5^{+} extra-embryonic ectoderm inclusion is not a transient state of all *Smad5* mutants, but represents a possible alternative consequence of a posterior amniotic ectoderm deficit in the absence of SMAD5.

Altered apoptosis, proliferation or ECM production are unlikely to cause the amniotic deficit

An amniotic ectoderm deficit could result from alterations in apoptosis or cell proliferation. TUNEL analysis revealed little cell death in mutant or control conceptuses with no evidence of increased apoptosis in mutants (Fig. S6), in agreement with apoptosis-related gene sets being unaltered in mutants in GSEA. Quantification of proliferation in the ectoderm of the amniochorionic fold by phospho-histone 3 (PH3) detection

Development (2018) 145, dev157222. doi:10.1242/dev.157222

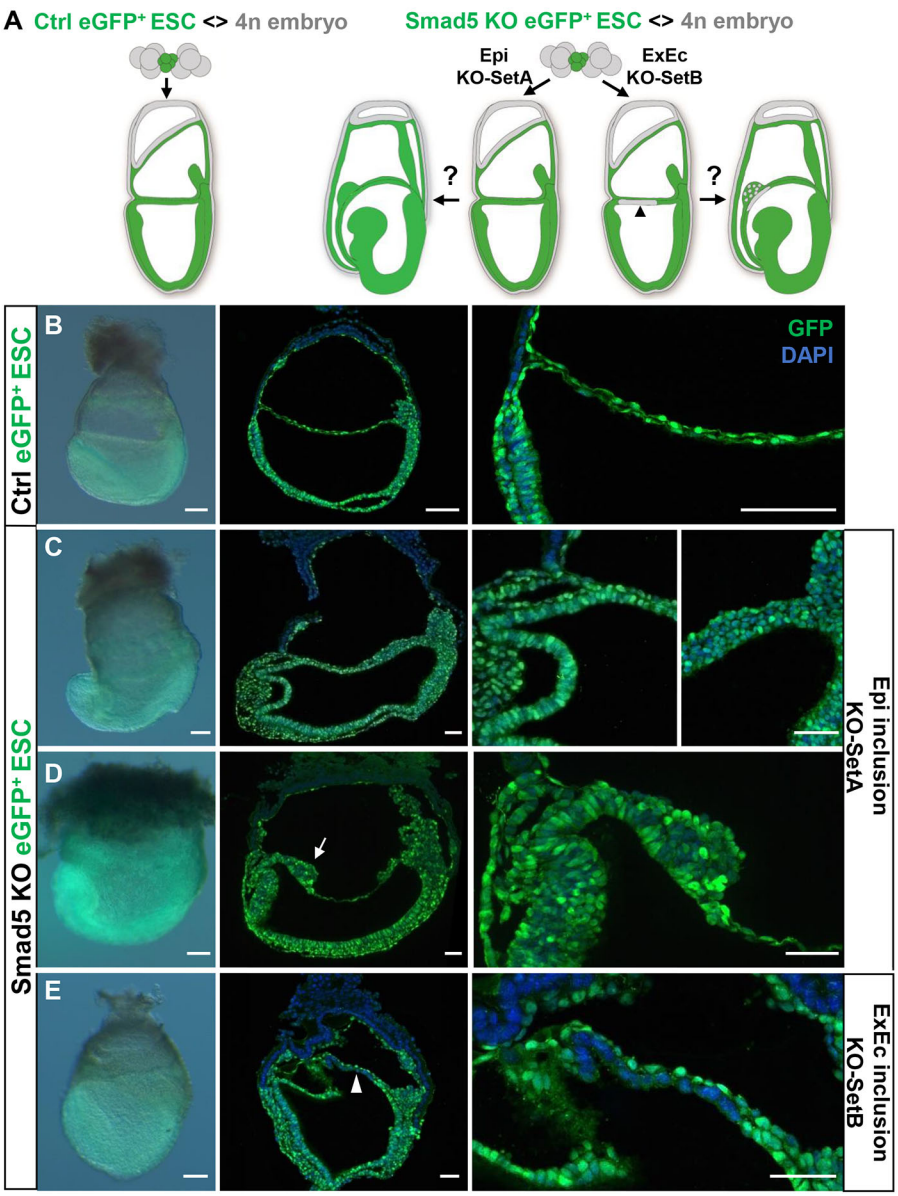

Fig. 7. Tetraploid chimera production confirms two separate amnion defects in *Smad5* mutants. (A) Morula aggregation of control *GFP*$^{+}$ *ESC*↔4n WT and *Smad5*$^{-/-}$*;GFP*$^{+}$ *ESC*↔4n WT assays with (potential) outcome. The mutant amnion can be completely epiblast (Epi) derived or can contain an extra-embryonic ectoderm (ExEc) inclusion (arrowhead). The latter would result in a GFP^{-} section in the mutant amnion that might or might not further transdifferentiate into the aggregate. (B-E) Chimeric embryos derived from GFP^{+} WT (B, E7.5) or *Smad5*$^{-/-}$ (C-E, left panels) ESCs; and longitudinal sections of the same embryos stained with anti-GFP antibody (green). See also Fig. S5. Epiblast ectoderm inclusion (C,D) as well as ExEc inclusion (E, arrowhead) were observed. Amniotic aggregates (D, arrow) were always GFP^{+}. Scale bars: 100 µm in whole mounts; 50 µm in sections.

revealed no significant difference in mitotic cells between control and knockout embryos (Fig. S7A,B).

Altered cell shape, ECM assembly and/or cell-cell and cell-matrix interactions could affect the squamous architecture and expansion of the amniotic ectoderm in mutants. GSEA analysis confirmed robust downregulation in ‘collagen and ECM’-related gene sets in mutants (Fig. S3B,C, Table S2). This differential expression could be caused by absence of SMAD5 in amniotic ectoderm, but could also reflect the relative under-representation of amniotic ectoderm over trapped nonamniotic tissue. We examined the spatial protein distribution of the ECM component collagen IV (ColIV). Normally, the ColIV matrix intertwined between amniotic ectoderm and mesoderm cells at E7.5 and E8.5 (Fig. S7A,B). In mutants, ColIV deposition seemed unaffected in regions in which the amnion was a smooth, thin bilayer. ColIV was, however, absent from ectoderm in regions with thickened amniotic ectoderm or an aggregate, and seemed only anchored by amniotic mesoderm (Fig. S7A,B). Postn, an ECM protein that directly interacts with fibronectin, collagen I (ColI) and ColIV (Conway et al., 2011; Horiuchi et al., 1999), had a similar distribution to ColIV in mutants (Fig. S7C). The differential presence of collagens and Postn in the amniotic aggregate supported amnion identity being partially affected. This might result from altered properties of the anterior amniotic ectoderm in controlling shape and stretchability (anterior amniotic ectoderm misdifferentiation), or inclusion of nonamniotic epiblast-derived tissue (epiblast inclusion).

DISCUSSION

Clonal analysis of normal amnion development showed that only a few descendants of some cells in a restricted area of the early proximal anterolateral epiblast contribute to amniotic ectoderm development. These descendants expand the amnion in distinct modes. Type I cells initiate amniotic ectoderm development and, together with Type II cells, expand this tissue from the posterior (Fig. 8A,B). Both originate in the epiblast adjacent to the extra-embryonic ectoderm, which is a potent source of BMP4 and BMP8B (Ying et al., 2000; Lawson et al., 1999), in a region that contributes to allantois, PGCs, extra-embryonic mesoderm and posterior embryonic mesoderm (Fig. 1; Lawson and Hage, 1994). Type I and II progenitors have co-descendants in exactly these posterior tissues, and all these tissues are delayed and reduced in

Development (2018) 145, dev157222. doi:10.1242/dev.157222

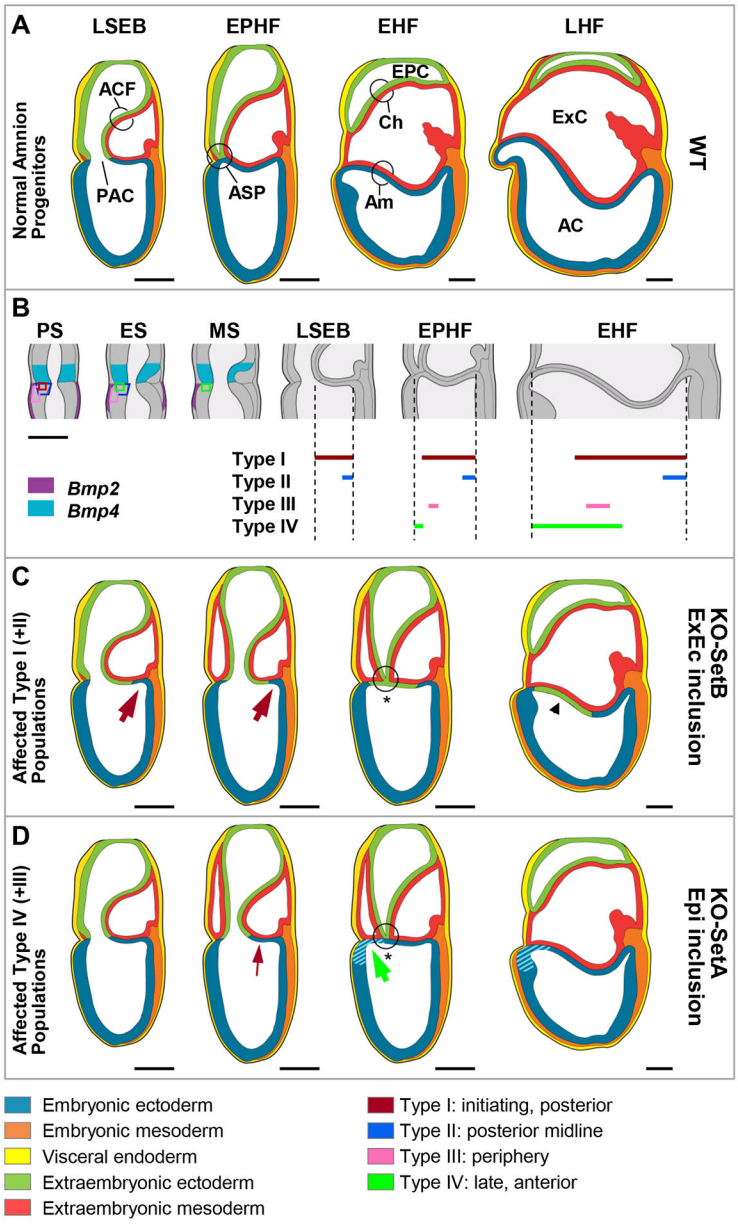

Fig. 8. Model of normal and abnormal amniogenesis. (A) Schematic representation of normal amnion expansion. (B) Expression of BMP ligands and spatiotemporal region of the progenitors of the different clone types contributing to amniotic ectoderm (regions in respective colour) at PS, ES and MS stages. *Bmp2* (Madabhushi and Lacy, 2011) and *Bmp4* (Lawson et al., 1999) are expressed in the three stages; the expression of *Bmp8b* (Ying and Zhao, 2001) in ExEc is only reported at ES (not shown). Representation of amniotic contribution of descendants of the four different clone types (Figs 2 and 3B). (C,D) Two sets of amnion defects occur in *Smad5* mutants. Posteriorized closure of the PAC and ASP (circle with asterisk) are common to both, indicating a deficiency in Type I descendants (burgundy arrows). In a few mutants (KO-SetB), a major deficiency in Type I, descendants, and presumably also a reduced Type II amniotic ectoderm contribution, causes an early posterior amniotic ectoderm deficiency leading to cuboidal chorionic extra-embryonic ectoderm trapping into the amniotic environment at PAC closure (arrowhead) (C). In most mutants (KO-SetA), the Type IV (and III) population is reduced (green arrow) with consequent inclusion of nonamniotic epiblast in amnion, or, alternatively, anterior amniotic ectoderm differentiation stalls, preventing the cuboidal-to-squamous transition of this epithelium (both represented by light-blue stripes) (D). In these mutants, the atypical ectoderm will transdifferentiate into an amniotic aggregate with posterior streak mesoderm features. Epiblast (D) and extra-embryonic inclusion (C) defects might occur together, but our data are not conclusive on this point. Scale bars: 100 µm. AC, amniotic cavity; ACF, amniochorionic fold; Am, amnion; ASP, anterior separation point; Ch, chorion; EHF, early headfold; EPC, ectoplacental cavity; EPHF, early preheadfold; ExC, exocoelomic cavity; LHF, late headfold; LSEB, late streak early allantoic bud; PAC, proamniotic canal.

Smad5 mutants (Bosman et al., 2006). Type III clones contribute facultatively, from the periphery, to amniotic ectoderm, and are derived from a region (presumptive surface ectoderm) that requires BMP signalling (Madabhushi and Lacy, 2011). Strikingly, Type IV progenitors reside in the epiblast spanning the anterior midline of the extra-embryonic–embryonic junction at ES+/MS, an area that is then precisely overlain by a restricted source of BMP2 in the anterior visceral endoderm (Madabhushi and Lacy, 2011). Overall, the identified progenitor regions are in close proximity to BMP sources, the relationship being closest for the very restricted, sequentially present Type I and IV progenitors that generate the bulk of the amniotic ectoderm.

When relating the clonal analysis results to the *Smad5* mutant embryo analyses (Fig. 8B-D), the consistently delayed and posteriorized proamniotic canal closure is compatible with a posterior amniotic ectoderm deficiency resulting from undersized

Table 2. Mutant chimeric phenotypes resulting from tetraploid complementation assay with Smad5 KO GFP$^+$ ESCs

		Epiblast inclusion without aggregate				Epiblast inclusion with aggregate					
Stage	ExEc inclusion	Head-out and thick AmEc	Thick AmEc	Head-out	Total epiblast inclusion	Anterior	Midline	Posterior	Total aggregate	Other[(1)]	Total
E7.5-E8.0	3	7	9	–	16	–	–	–	–	2	21
E8.5>4S	–	1	–	4	5	1	2	3	6	3	14
Total	3 (9%)	8	9	4	21 (60%)	1	2	3	6 (17%)	5 (14%)	35

[(1)]Other: two chimeras without visible amnion; two chimeras with control phenotype; one very small embryo.
AmEc, amniotic ectoderm; ExEc, extra-embryonic ectoderm.

Development (2018) 145, dev157222. doi:10.1242/dev.157222

or delayed BMP4-dependent amniotic ectoderm founding population(s) [Type I (and II)]. The inclusion of chorionic extra-embryonic ectoderm in the amniotic environment of KO-SetB and some tetraploid chimeras showed that the trailing chorionic portion of the amniochorionic fold might become trapped in the amnion at proamniotic canal closure (Fig. 8C).

In the majority of the mutants, the KO-SetA mutants, the phenotype seems to implicate primarily the Type IV group (Fig. 8D). In these mutants, the anterior extra-embryonic–embryonic border is obscure, and the anterior ectoderm is nonsquamous. One possibility is that the Type IV progenitor population expands normally in the amniotic ectoderm territory but fails to acquire the typical expanded squamous morphology of amniotic epithelium. Alternatively, under-representation of Type IV descendants is compensated by inclusion of neighbouring anterior surface ectoderm into the amniotic environment. The RNA-seq analysis did not directly support such an event as there was no major differential expression of surface ectoderm markers, such as *Dlx5* or *Aldh1a3* (Qu et al., 2016); however, low abundant transcripts might have been under-represented in our study. Conversely, the persistent expression of the early epiblast marker *Fgf5* in the anterior extra-embryonic–embryonic junction region of the mutants is suggestive of a stalled epiblast differentiation (atypical anterior ectoderm). In the absence of specific molecular markers of amniotic ectoderm in ES/MS embryos, the answer to whether the KO-SetA signature tissue is caused by misdifferentiated Type IV descendants or atypical surface ectoderm could potentially be obtained from prospective lineage analyses at ES+ to LS stages in *Smad5* mutants.

Further support for SMAD5 being a major signal mediator of BMP2 in the proximal anterolateral region of the embryo comes from mice that lack *Bmp2* ubiquitously or conditionally in the anterior visceral endoderm (Zhang and Bradley, 1996; Madabhushi and Lacy, 2011). Such embryos show defects that are reminiscent of and equally variable as those in *Smad5* mutants (Bosman et al., 2006; Chang et al., 1999) and tetraploid chimeras; i.e. proamniotic canal closure defects, severely impaired anterior midline epiblast tissues and ventral folding morphogenesis defects. However, an aggregate with posterior streak mesoderm potency in the anterior part of the amnion seems to form exclusively in *Smad5* mutants. This suggests that SMAD5 deficiency compromises additional BMP signalling pathways, e.g. BMP4, but potentially also BMP5 that is produced in embryonic mesoderm flanking the anterior extra-embryonic–embryonic interface (Solloway and Robertson, 1999). Alternatively, intracellular non-SMAD5 cascades could be disturbed. Indeed, in cell culture experiments, loss of SMAD5 can result in gain of Nodal-SMAD2/3 signalling (Pereira et al., 2012). Indications of such alterations in the *Smad5* mutants are the robust ectopic expression of *Nodal* and gain of Nodal signalling (expression of Nodal-SMAD2/3 target genes *Lefty2*, *Eomes*, *Cripto*, *Wnt3*) in the nonsquamous cells in anterior amniotic ectoderm (Pereira et al., 2012) and in the KO-SetA RNA-seq results.

The chimera study showed that the amniotic aggregate is of epiblast origin, thus excluding that extra-embryonic ectoderm inclusions (KO-SetB) transdifferentiate into an aggregate with characteristics of posterior streak mesoderm (KO-SetA mutants). However, the intermediate expression of selected KO-SetB and KO-SetA markers in some mutant amnion samples (8/25) is compatible with ‘mixed’ or variable phenotypes. Whether a mutant develops into a SetA or SetB phenotype, or ‘anterior’ and ‘posterior’ amniotic ectoderm defects co-exist, might be a stochastic event. When the amniotic ectoderm does not stretch fast enough around the time of proamniotic canal closure, the mechanical forces at the extra-embryonic–embryonic interface that balance turgor in the exocoelom and (pro)amniotic cavities might ‘drag’ tissue from the conceptus into the amniotic ectoderm from wherever there is least resistance (as normally in Type III clone behaviour). Interestingly, an extra-embryonic ectoderm inclusion in the amnion has also been described for *Pagr1a* knockouts (Kumar et al., 2014). *Pagr1a* encodes a protein associated with PAX-interacting protein 1 (Paxip1) and is predominantly expressed in the chorion. Its absence results in downregulation of *Bmp2* in the anterior extra-embryonic–embryonic junction.

The driving force behind the cuboidal-to-squamous transition of amniotic ectoderm still remains unclear. Interestingly, BMP-SMAD signalling has been reported as a driver of organogenesis by regulating cell shape and interpreting mechanical forces at the tissue level (Nerurkar et al., 2017; Poduri et al., 2017; Wang et al., 2012). It is likely that the increase in turgor associated with the dynamic expansion of the exocoelomic and amniotic cavities, the folding morphogenesis of the embryo following amnion-chorion separation, and/or alterations in cell-matrix and cell-cell interactions each contribute to significant changes in cytoskeletal rearrangements. Our study relates BMP-SMAD signalling to these events in the amniotic ectoderm.

Collectively, the amnion RNA-seq approach and chimera study have shown that SMAD5 mediates spatial cues crucial for the establishment of the amniotic ectoderm. The founding population of the amniotic ectoderm in mouse embryos deficient in SMAD5 is probably too small or delayed, and the stalled cuboidal-to-squamous transition of anterior amniotic ectoderm does not keep pace with exocoelom expansion and axial growth, hindering ventral folding morphogenesis. The complex and variable amnion phenotypes can be attributed to SMAD5 loss of function affecting different progenitor populations for amniotic ectoderm. These arise sequentially from a distinct region of the anterior proximal epiblast exposed to BMP4 and BMP2, and expand amniotic ectoderm initially posteriorly and then from the anterior. Our study also supports a new role for the flexible amnion, in addition to its known protective function, one in accommodating the shaping of the embryo proper.

MATERIALS AND METHODS

Embryo culture, single-cell labelling and clone plotting

[C57BL6×CBA.Ca] F1 and F2, and some Dub:ICR mouse (*Mus musculus*) embryos were used (Table S6). Terminology of embryo staging was as in Lawson and Wilson (2015). For the nominal age at injection, embryonic day was counted, with E0 being the middle of the dark period during overnight mating; 0.1 day was subtracted to allow for the developmental delay as a result of dissection and labelling. Culture of E6 PS stage and E6.5 ES stage embryos and the iontophoretic injection of single epiblast cells were as reported previously (Beddington and Lawson, 1990; Lawson et al. 1991; Perea-Gomez et al. 2001). In brief, clones were generated by iontophoretically injecting one epiblast cell/embryo with either a mixture of 7.4% horse radish peroxidase (HRP, EIA grade, 10814407001, Roche) and 2.6% lysinated rhodamine dextran (LRDX, M_r 10×10^3, D1817, Molecular Probes) or with 10% LRDX alone, both in 0.05 M KCl, using 1-3 nA depolarising current for 10-20 s, with a duty cycle of 500 ms/s and frequency of 1 s. An additional injection of 5-10 s into an extra-embryonic visceral endoderm cell in the same focal plane provided a marker clone in the same radial position as the injected epiblast cell. Embryos were cultured for 1 day or 1.5+ days, stained for HRP where relevant, fixed with 5% paraformaldehyde in PBS, dehydrated and cleared in BABB, when labelled cells were counted. The location and number of labelled cells were confirmed on 7 µm serial sections of the material embedded in glycol methacrylate (Technovit). PGCs were identified on the basis of their characteristic pattern of alkaline phosphatase activity, in sections of embryos labelled only with LRDX (Ginsburg et al., 1990; Lawson and Hage, 1994).

Development (2018) 145, dev157222. doi:10.1242/dev.157222

Clonal descendants in the amniotic ectoderm were plotted on an appropriate template using information from the whole mount and sections to normalize the plot. Amnion templates were derived from 3D embryo reconstructions in the eMouseAtlas (Armit et al., 2017), specifically EMA:224 (TS 10b, LSEB/EPHF), EMA:17 (TS 11, LPHF/EHF), EMA:220 (TS 12a, 2S) and EMA:218 (TS 12b, 5S). Templates were created from measurements over the surface of the amnion in both sagittal and frontal orientation. Because of the extreme curvature of the amnion by the 5S stage, the 2D template for this stage is a compromise between the linear dimensions over the surface and the shorter periphery of the base of a dome. Template dimensions were adjusted for 20% shrinkage during histological processing of the embryos used in the eMouseAtlas.

Smad5 mutant mouse strain, microdissection and genotyping

Smad5-deficient mouse embryos (within decidua or isolated) from heterozygous *Smad5*$^{-/+}$ crosses (*Smad5*^{tm1Zuk}) (Chang et al., 1999) of mixed C57BL/6J×CBA background were collected in ice-cold PBS at E7.5-E8.5. Amnion was stepwise microsurgically isolated from EPHF- to 2S-stage embryos using tungsten needles as shown in Fig. 4C,D, and frozen on dry ice. PCR genotyping was performed on leftover embryonic material. For genotyping of embryos sectioned within the decidua, side sections were mounted on PALM membrane slides (415190-9041-000, Zeiss), stained with Cresyl Violet and subjected to laser capture microdissection (LCM) on a PALM MicroBeam laser capture system (Zeiss) to isolate embryonic tissue for genotyping. DNA for PCR was isolated after on-cap lysis in LCM lysis buffer (0.5 M EDTA pH 8.0, 1 M Tris pH 8.0 and Igepal CA-630). Sex was determined by Jarid1c (Kdm5c)/Jarid1d (Kdm5d) and Sry/IL3 PCR (Table S7). In all experiments, stage-matched Smad5$^{-/+}$ or Smad5$^{+/+}$ littermates were used as controls to Smad5$^{-/-}$ embryos. All animal experiments were approved by the ethical commission of KU Leuven (P097/2008; P077/2014; P251/2014). The care and use of mice complied with the national and institutional regulatory standards of the Hubrecht Laboratory (The Netherlands), The University of Edinburgh (UK) and KU Leuven (Belgium).

RT-qPCR

Primers for RT-qPCR on cDNA from single amnion samples (Table S7) were designed in maximal proximity to the 3′ ends of target transcripts, to compensate for the potential 3′ bias that might be generated during amplification (see 'Single amnion cDNA amplification' section). Samples were processed on a LightCycler480 Real-Time PCR System with LightCycler 480 SYBRGreen I Master Mix (Roche, 4707516001) in technical duplicates. Reference genes for amniotic tissue were chosen using GeNorm. For the analysis in Fig. 5D, expression was normalized to two reference genes – Gapdh and Psmd4 – using the ΔΔCt method and qbase+ software (Biogazelle). For the analysis shown in Fig. S3A, expression was normalized to Psmd4, and presented with the ΔCt method, which reflects the Ct difference between the reference and the test transcript (in Fig. S3A, the higher ΔCt, the higher the expression).

Single amnion cDNA amplification

cDNA for RT-qPCR and RNA-seq was prepared from individual E7.5 amnions and amplified following adaptation of a procedure originally designed for RNA-seq of single-cells (Tang et al., 2009) on the SOLiD platform ('Double-stranded cDNA synthesis from a single cell', Applied Biosystems demonstrated protocol). Briefly, reverse transcription and second-strand cDNA synthesis was performed in the sample lysate without RNA isolation, using SuperScript III Reverse Transcriptase (Invitrogen) and poly-dT universal primers. This was followed by two rounds of PCR amplification (18 and 12 cycles, respectively) and column purifications (QIAquick, Qiagen), generating up to 3 kb coverage at the 3′ end of all poly-adenylated transcripts. The resulting cDNA was used for RT-qPCR and RNA-seq. The cDNA yield for the 12 RNA-seq samples is shown in Table S1.

Whole transcriptome sequencing and bioinformatics analysis

Between 30 and 60 million reads were generated per library; 20%-27% of them mapped uniquely to the genome (Table S1). Raw colorspace reads were mapped to the mouse genome GRCm38.83 with TopHat2 software (v2.1.1) (Kim et al., 2013; Trapnell et al., 2009) using colorspace compatible parameters: Bowtie 1 (v1.1.2.0), –color –quals and coverage-search algorithm. Transcript coordinates were extracted from the Genome Reference Center reference annotation with Gffread from the Cufflinks v2.1.1 suite and merged to gene coordinates with mergeBed from the Bedtools v2.17.0 toolkit (Kim et al., 2013; Quinlan and Hall, 2010; Trapnell et al., 2011). GC content and gene length were derived from the gene coordinates. The numbers of aligned reads per gene were summarized using featureCounts v1.5.3 with parameters '-Q 0 -s 0 -t exon -g gene id' (Liao et al., 2014). We removed 22,528 genes for which all samples had less than 1 count per million. As such, we continued with raw counts for 16,033 genes.

Raw counts were imported in R package DESeq2 1.18.1 (Love et al., 2014) for library size normalization and differential expression analyses. The counts were subjected to variance stabilizing transformation (VST) (Anders and Huber, 2010). The variance normalized counts were used for gene expression visualization and clustering. Clustering of all 12 samples was performed by principal component analysis (PCA). In DESeq2, a negative binomial generalized linear model (GLM) was fitted against the normalized counts. Differential expression was tested for with a Wald statistical test, also implemented in the DESeq2 package. The resulting *P*-values were corrected for multiple testing with Benjamini–Hochberg to control the false discovery rate (FDR). Differentially expressed genes were further filtered using FDR≤0.05 and |log2 FC|≥1. Expression heat maps were generated in MultiExperiment Viewer (MeV) using VST values. GSEA analysis is described in the Supplementary Materials and Methods.

Immunohistochemistry, TUNEL assay and whole-mount *in situ* hybridization

Embryos and decidua were fixed overnight in 4% paraformaldehyde in PBS, embedded in paraffin and sectioned at 6 µm. Fixed chimeric embryos were pre-embedded in 1.5% agarose prior to paraffin embedding and sectioning. Fluorescent and chromogenic antibody staining was performed on an automated platform (Ventana Discovery, Ventana Medical Systems) or manually using standard procedures. We used antibodies raised against Oct3/4 (1:100, ab19857), Eomes (1:250, ab23345), collagen IV (1:100, ab6586), phospho-histone 3 (1:100, ab5176) and GFP (1:100, ab13970) from Abcam; and Elf5 (1:40, sc-9645) and periostin (1:100, sc-67233) from Santa Cruz Biotechnology. Differently labelled secondary antibodies raised in donkey or goat were used (1:300, Jackson ImmunoResearch). Omitting the primary antibody served as a negative control. Nuclei were counterstained with DAPI (1:1000, D3571, Invitrogen) or Haematoxylin. TUNEL assay was performed using a Fluorescein *In Situ* Cell Death Detection kit (Roche) according to the manufacturer's instructions. Proliferation data were statistically analysed with Prims 6 software (GraphPad). The nonparametric Mann–Whitney *U*-test was used for comparisons of the two groups.

Whole-mount *in situ* hybridization was performed as previously described (Pereira et al., 2011). The *Fgf5* cDNA template used for riboprobe synthesis and digoxigenin labelling was generated by PCR (Table S7). Probe hybridization was at 60°C.

Tetraploid complementation assay and generation of chimeric embryos

Chimeric embryos were produced as described (Eakin and Hadjantonakis, 2006). Briefly, tetraploidy was achieved by electrofusion of two-cell stage CD1 embryos. WT and *Smad5* knockout mouse ESCs (Bosman et al., 2006) were transduced with lentivirus containing *eGFP* gene under the control of elongation factor 1 alpha promoter. Two tetraploid zona pellucida-free morula embryos were aggregated with GFP^{+} ESCs to produce either *Smad5*$^{-/-}$*;GFP*$^{+}$ ESC↔4n WT or *WT;GFP*$^{+}$ ESC↔4n WT chimeras, respectively knockout and WT chimeras. Blastocysts were transferred into the uteri of pseudopregnant females. Embryos were microdissected, imaged for GFP fluorescence and fixed. In total, 35 knockout and five WT chimeras were embedded in agarose and paraffin. Sections were subjected to immunofluorescence against GFP.

Acknowledgements
We are grateful to Z. Zhang and L. Vermeire for chimera production; R. Janky and VIB Nucleomics Core (www.nucleomics.be) for mapping and bioinformatics analysis; A. Francis, E. Seuntjens and E. Radaeli for immunosupport (InfraMouse, Hercules infrastructure ZW09-03); C. Hertz-Fowler's team (Liverpool) for SOLiD sequencing; J. Korving and P. Lanser for methacrylate sections, E. Maas for mouse husbandry; C. Verfaillie for the lentiviral unit; and A. Camus, M. Bialecka, R. Dries, L. Umans and D. Davidson for discussions.

Competing interests
The authors declare no competing or financial interests.

Author contributions
Conceptualization: M.P.D., K.A.L., A.Z.; Methodology: M.P.D., V.A.E., K.A.L., A.S., S.A., A.Z.; Software: M.N.S., S.A.; Validation: M.P.D., V.A.E., K.A.L., M.N.S., S.A.; Formal analysis: M.P.D., V.A.E., K.A.L., M.N.S., S.A., A.Z.; Investigation: M.P.D., V.A.E., K.A.L., L.C.P., P.N.G.P., A.S., N.C., S.M.C.d.S.L.; Resources: D.H., S.M.C.d.S.L.; Data curation: M.P.D., V.A.E., K.A.L., M.N.S., S.A., A.Z.; Writing - original draft: M.P.D., K.A.L., A.Z.; Writing - review & editing: M.P.D., V.A.E., K.A.L., M.N.S., L.C.P., P.N.G.P., A.S., N.C., D.H., S.M.C.d.S.L., S.A., A.Z.; Visualization: M.P.D., V.A.E., K.A.L., L.C.P., N.C., A.Z.; Supervision: A.Z.; Project administration: A.Z.; Funding acquisition: D.H., S.A., A.Z.

Funding
This work was supported by Vlaams Instituut voor Biotechnologie (VIB) and VIB TechWatch, Belspo [IUAP-6/20 and 7/07], the Medical Research Council and Koninklijke Nederlandse Akademie van Wetenschappen. M.P.D. was a VIB predoctoral fellow. Deposited in PMC for release after 6 months.

Data availability
RNA-seq data are available at Gene Expression Omnibus (GEO), under accession number GSE99211.

Supplementary information
Supplementary information available online at
http://dev.biologists.org/lookup/doi/10.1242/dev.157222.supplemental

References

Anders, S. and Huber, W. (2010). Differential expression analysis for sequence count data. *Genome Biol.* **11**, R106.
Armit, C., Richardson, L., Venkataraman, S., Graham, L., Burton, N., Hill, B., Yang, Y. and Baldock, R. A. (2017). eMouseAtlas: an atlas-based resource for understanding mammalian embryogenesis. *Dev. Biol.* **423**, 1-11.
Arnold, S. J., Hofmann, U. K., Bikoff, E. K. and Robertson, E. J. (2008). Pivotal roles for eomesodermin during axis formation, epithelium-to-mesenchyme transition and endoderm specification in the mouse. *Development* **135**, 501-511.
Beddington, R. S. P. and Lawson, K. A. (1990). Clonal analysis of cell lineage. In *Postimplantation Mammalian Embryos: A Practical Approach* (ed. A. J. Copp and D. L. Cockroft), pp. 267-316. Oxford: IRL Press.
Bosman, E. A., Lawson, K. A., Debruyn, J., Beek, L., Francis, A., Schoonjans, L., Huylebroeck, D. and Zwijsen, A. (2006). Smad5 determines murine amnion fate through the control of bone morphogenetic protein expression and signalling levels. *Development* **133**, 3399-3409.
Cajal, M., Lawson, K. A., Hill, B., Moreau, A., Rao, J., Ross, A., Collignon, J., Camus, A., Acampora, D., Merlo, G. R. et al. (2012). Clonal and molecular analysis of the prospective anterior neural boundary in the mouse embryo. *Development* **139**, 423-436.
Cajal, M., Creuzet, S. E., Papanayotou, C., Sabéran-Djoneidi, D., Chuva de Sousa Lopes, S. M., Zwijsen, A., Collignon, J. and Camus, A. (2014). A conserved role for non-neural ectoderm cells in early neural development. *Development* **141**, 4127-4138.
Chang, H., Huylebroeck, D., Verschueren, K., Guo, Q., Matzuk, M. M. and Zwijsen, A. (1999). Smad5 knockout mice die at mid-gestation due to multiple embryonic and extraembryonic defects. *Development* **126**, 1631-1642.
Ciruna, B. G. and Rossant, J. (1999). Expression of the T-box gene Eomesodermin during early mouse development. *Mech. Dev.* **81**, 199-203.
Conway, S. J., Doetschman, T. and Azhar, M. (2011). The inter-relationship of periostin, TGF beta, and BMP in heart valve development and valvular heart diseases. *ScientificWorldJournal* **11**, 1509-1524.
de Melo Bernardo, A. and Chuva de Sousa Lopes, S. M. (2014). The involvement of the proamnion in the development of the anterior amnion fold in the chicken. *PLoS ONE* **9**, e92672.
Dobreva, M. P., Lhoest, L., Pereira, P. N. G., Umans, L., Camus, A., Chuva de Sousa Lopes, S. M. and Zwijsen, A. (2012). Periostin as a biomarker of the amniotic membrane. *Stem Cells Int.* **2012**, 1-10.
Donnison, M., Beaton, A., Davey, H. W., Broadhurst, R., L'Huillier, P. and Pfeffer, P. L. (2005). Loss of the extraembryonic ectoderm in Elf5 mutants leads to defects in embryonic patterning. *Development* **132**, 2299-2308.
Downs, K. M. (2008). Systematic localization of oct-3/4 to the gastrulating mouse conceptus suggests manifold roles in mammalian development. *Dev. Dyn.* **237**, 464-475.
Eakin, G. S. and Hadjantonakis, A.-K. (2006). Production of chimeras by aggregation of embryonic stem cells with diploid or tetraploid mouse embryos. *Nat. Protoc.* **1**, 1145-1153.
Egea, J., Erlacher, C., Montanez, E., Burtscher, I., Yamagishi, S., Hess, M., Hampel, F., Sanchez, R., Rodriguez-Manzaneque, M. T., Bosl, M. R. et al. (2008). Genetic ablation of FLRT3 reveals a novel morphogenetic function for the anterior visceral endoderm in suppressing mesoderm differentiation. *Genes Dev.* **22**, 3349-3362.
Ginsburg, M., Snow, M. and McLaren, A. (1990). Primordial germ cells in the mouse embryo during gastrulation. *Development* **110**, 521-528.
Horiuchi, K., Amizuka, N., Takeshita, S., Takamatsu, H., Katsuura, M., Ozawa, H., Toyama, Y., Bonewald, L. F. and Kudo, A. (1999). Identification and characterization of a novel protein, periostin, with restricted expression to periosteum and periodontal ligament and increased expression by transforming growth factor β. *J. Bone Miner. Res.* **14**, 1239-1249.
Horn, T. and Panfilio, K. A. (2016). Novel functions for *Dorsocross* in epithelial morphogenesis in the beetle *Tribolium castaneum*. *Development* **143**, 3002-3011.
Imuta, Y., Koyama, H., Shi, D., Eiraku, M., Fujimori, T. and Sasaki, H. (2014). Mechanical control of notochord morphogenesis by extra-embryonic tissues in mouse embryos. *Mech. Dev.* **132**, 44-58.
Inai, K., Norris, R. A., Hoffman, S., Markwald, R. R. and Sugi, Y. (2008). BMP-2 induces cell migration and periostin expression during atrioventricular valvulogenesis. *Dev. Biol.* **315**, 383-396.
Katagiri, T. and Watabe, T. (2016). Bone morphogenetic proteins. *Cold Spring Harbor Perspect. Biol.* **8**, a021899.
Kim, D., Pertea, G., Trapnell, C., Pimentel, H., Kelley, R. and Salzberg, S. L. (2013). TopHat2: Accurate alignment of transcriptomes in the presence of insertions, deletions and gene fusions. *Genome Biol.* **14**, R36.
Kinder, S. J., Tsang, T. E., Wakamiya, M., Sasaki, H., Behringer, R. R., Nagy, A. and Tam, P. P. (2001). The organizer of the mouse gastrula is composed of a dynamic population of progenitor cells for the axial mesoderm. *Development* **128**, 3623-3634.
Kumar, A., Lualdi, M., Loncarek, J., Cho, Y.-W., Lee, J.-E., Ge, K. and Kuehn, M. R. (2014). Loss of function of mouse Pax-Interacting Protein 1-associated glutamate rich protein 1a (Pagr1a) leads to reduced Bmp2 expression and defects in chorion and amnion development. *Dev. Dyn.* **243**, 937-947.
Lawson, K. A. and Hage, W. J. (1994). Clonal analysis of the origin of primordial germ cells in the mouse. *Ciba Foundation Symp.* **182**, 68-84-91.
Lawson, K. A. and Wilson, V. A. (2015). Revised staging of mouse development before organogenesis. In *Kaufman's Atlas of Mouse Development Supplement* (ed. R. Baldock, J. Bard, D. R. Davidson and G. Morris-Kay), pp. 51-64. Amsterdam, The Netherlands: Elsevier.
Lawson, K. A., Meneses, J. J. and Pedersen, R. A. (1991). Clonal analysis of epiblast fate during germ layer formation in the mouse embryo. *Development* **113**, 891-911.
Lawson, K. A., Dunn, N. R., Roelen, B. A. J., Zeinstra, L. M., Davis, A. M., Wright, C. V. E., Korving, J. P. W. F. M. and Hogan, B. L. M. (1999). Bmp4 is required for the generation of primordial germ cells in the mouse embryo. *Genes Dev.* **13**, 424-436.
Li, L., Liu, C., Biechele, S., Zhu, Q., Song, L., Lanner, F., Jing, N. and Rossant, J. (2013). Location of transient ectodermal progenitor potential in mouse development. *Development* **140**, 4533-4543.
Liao, Y., Smyth, G. K. and Shi, W. (2014). FeatureCounts: An efficient general purpose program for assigning sequence reads to genomic features. *Bioinformatics* **30**, 923-930.
Love, M. I., Huber, W. and Anders, S. (2014). Moderated estimation of fold change and dispersion for RNA-seq data with DESeq2. *Genome Biol.* **15**, 1-21.
Madabhushi, M. and Lacy, E. (2011). Anterior visceral endoderm directs ventral morphogenesis and placement of head and heart via BMP2 expression. *Dev. Cell* **21**, 907-919.
Menon, R. and Richardson, L. S. (2017). Preterm prelabor rupture of the membranes: A disease of the fetal membranes. *Semin. Perinatol.* **41**, 409-419.
Mesnard, D. and Constam, D. B. (2010). Imaging proprotein convertase activities and their regulation in the implanting mouse blastocyst. *J. Cell Biol.* **191**, 129-139.
Nerurkar, N. L., Mahadevan, L. and Tabin, C. J. (2017). BMP signaling controls buckling forces to modulate looping morphogenesis of the gut. *Proc. Natl Acad. Sci. USA* **114**, 2277-2282.
Opitz, J. M., Johnson, D. R. and Gilbert-Barness, E. F. (2015). ADAM "sequence" part II: hypothesis and speculation. *Am. J. Med. Genet. A* **167**, 478-503.
Perea-Gomez, A., Lawson, K. A., Rhinn, M., Zakin, L., Brûlet, P., Mazan, S. and Ang, S. L. (2001). Otx2 is required for visceral endoderm movement and for the restriction of posterior signals in the epiblast of the mouse embryo. *Development* **128**, 753-765.

Pereira, P. N. G., Dobreva, M. P., Graham, L., Huylebroeck, D., Lawson, K. A. and Zwijsen, A. N. (2011). Amnion formation in the mouse embryo: the single amniochorionic fold model. *BMC Dev. Biol.* **11**, 48.

Pereira, P. N. G., Dobreva, M. P., Maas, E., Cornelis, F. M., Moya, I. M., Umans, L., Verfaillie, C. M., Camus, A., de Sousa Lopes, S. M. C., Huylebroeck, D. et al. (2012). Antagonism of Nodal signaling by BMP/Smad5 prevents ectopic primitive streak formation in the mouse amnion. *Development* **139**, 3343-3354.

Poduri, A., Raftrey, B., Chang, A. H., Rhee, S., Van, M. and Red-Horse, K. (2017). Endothelial cells respond to the direction of mechanical stimuli through SMAD signaling to regulate coronary artery size. *Development* **144**, 3241-3252.

Qu, Y., Zhou, B., Yang, W., Han, B., Yu-Rice, Y., Gao, B., Johnson, J., Svendsen, C. N., Freeman, M. R., Giuliano, A. E. et al. (2016). Transcriptome and proteome characterization of surface ectoderm cells differentiated from human iPSCs. *Sci. Rep.* **6**, 32007.

Quinlan, A. R. and Hall, I. M. (2010). BEDTools: a flexible suite of utilities for comparing genomic features. *Bioinformatics* **26**, 841-842.

Rafiqi, A. M., Park, C.-H., Kwan, C. W., Lemke, S. and Schmidt-Ott, U. (2012). BMP-dependent serosa and amnion specification in the scuttle fly Megaselia abdita. *Development* **139**, 3373-3382.

Sasaki, K., Nakamura, T., Okamoto, I., Yabuta, Y., Iwatani, C., Tsuchiya, H., Seita, Y., Nakamura, S., Shiraki, N., Takakuwa, T. et al. (2016). The germ cell fate of cynomolgus monkeys is specified in the nascent amnion. *Dev. Cell* **39**, 169-185.

Schmidt, W. (1992). The amniotic fluid compartment: the fetal habitat. *Adv. Anat. Embryol. Cell Biol.* **127**, 1-100.

Shao, Y., Taniguchi, K., Gurdziel, K., Townshend, R. F., Xue, X., Yong, K. M. A., Sang, J., Spence, J. R., Gumucio, D. L. and Fu, J. (2016). Self-organized amniogenesis by human pluripotent stem cells in a biomimetic implantation-like niche. *Nat. Mater.* **16**, 419-425.

Solloway, M. J. and Robertson, E. J. (1999). Early embryonic lethality in Bmp5; Bmp7 double mutant mice suggests functional redundancy within the 60A subgroup. *Development* **126**, 1753-1768.

Tang, F., Barbacioru, C., Wang, Y., Nordman, E., Lee, C., Xu, N., Wang, X., Bodeau, J., Tuch, B. B., Siddiqui, A. et al. (2009). mRNA-Seq whole-transcriptome analysis of a single cell. *Nat. Methods* **6**, 377-382.

Tomás, A. R., Certal, A. C. and Rodríguez-León, J. (2011). FLRT3 as a key player on chick limb development. *Dev. Biol.* **355**, 324-333.

Trapnell, C., Pachter, L. and Salzberg, S. L. (2009). TopHat: discovering splice junctions with RNA-Seq. *Bioinformatics* **25**, 1105-1111.

Trapnell, C., Williams, B. A., Pertea, G., Mortazavi, A., Kwan, G., van Baren, M. J., Salzberg, S. L., Wold, B. J. and Pachter, L. (2011). Transcript assembly and quantification by RNA-Seq reveals unannotated transcripts and isoform switching during cell differentiation. *Nat. Biotechnol.* **28**, 511-515.

Wang, Y.-K., Yu, X., Cohen, D. M., Wozniak, M. A., Yang, M. T., Gao, L., Eyckmans, J. and Chen, C. S. (2012). Bone Morphogenetic protein-2-induced signaling and osteogenesis is regulated by cell shape, RhoA/ROCK, and cytoskeletal tension. *Stem Cells Dev.* **21**, 1176-1186.

Yang, X., Castilla, L. H., Xu, X., Li, C., Gotay, J., Weinstein, M., Liu, P. P. and Deng, C. X. (1999). Angiogenesis defects and mesenchymal apoptosis in mice lacking SMAD5. *Development* **126**, 1571-1580.

Ying, Y. and Zhao, G.-Q. (2001). Cooperation of endoderm-derived BMP2 and extraembryonic ectoderm-derived BMP4 in primordial germ cell generation in the mouse. *Dev. Biol.* **232**, 484-492.

Ying, Y., Liu, X.-M., Marble, A., Lawson, K. A. and Zhao, G.-Q. (2000). Requirement of *Bmp8b* for the generation of primordial germ cells in the mouse. *Mol. Endocrinol.* **14**, 1053-1063.

Zhang, H. and Bradley, A. (1996). Mice deficient for BMP2 are nonviable and have defects in amnion/chorion and cardiac development. *Development* **122**, 2977-2986.